2021

THE APPLICATION OF LEAKY WAVE ANTENNAS FOR MEDICAL HYPERTHERMIA TREATMENT AND BEAMFORMER IN FMCW AUTOMOTIVE RADAR SYSTEMS

Masoud Sarabi
Michigan Technological University, msarabi@mtu.edu

THE APPLICATION OF LEAKY WAVE ANTENNAS FOR MEDICAL HYPERTHERMIA TREATMENT AND BEAMFORMER IN FMCW AUTOMOTIVE RADAR SYSTEMS

By

Masoud Sarabi

A DISSERTATION

Submitted in partial fulfillment of the requirements for the degree of

DOCTOR OF PHILOSOPHY

In Electrical Engineering

MICHIGAN TECHNOLOGICAL UNIVERSITY

2021

This dissertation has been approved in partial fulfillment of the requirements for the Degree of DOCTOR OF PHILOSOPHY in Electrical Engineering.

Department of Electrical and Computer Engineering

Dissertation Advisor:	*Dr. Warren Perger*
Committee Member:	*Dr. Durdu Guney*
Committee Member:	*Dr. Tony Pinar*
Committee Member:	*Dr. Ramy El-Ganainy*
Department Chair:	*Dr. Glen Archer*

Dedication

To my most dear mother Maryam Mobarraz Haghighi who taught me patience and perseverance in life

&

In memory of my beloved father Ali Sarabi who never got to see this but he is on every page

Table of Contents

Author Contribution Statement

This dissertation is the presented works of 5 interdependent chapters one of which is published in Texas Symposium on Wireless and Microwave Circuits and Systems, (WMCS) and two other chapters are originated from two journal papers, one under review and another one under submission. All the work has been done by myself.

Masoud Sarabi

The papers are:

1) M. Sarabi and W. Perger, "A Novel Leaky Wave Antenna for hyperthermia," 2019 IEEE Texas Symposium on Wireless and Microwave Circuits and Systems (WMCS), 2019, pp. 1-4, doi: 10.1109/WMCaS.2019.8732516.

2) M. Sarabi and W. Perger, “Possible Leaky Wave Antennas for Propagation Therapy Using SAR Analysis”, Under review in Applied Computational Electromagnetics Society, March, 2021.

3) M. Sarabi and W. Perger, “A novel 77 GHz FMCW comb-line leaky wave antenna for automotive radar system”, Submitted to IEEE Transactions on Antennas & Propagation, July, 2021.

Abstract

Thousands of years ago human discovered that if a slice of amber is rubbed against fur, it would absorb light-weight objects. Hundreds of years after that the ancient people figured out that there are actually two different characteristics of attraction and repulsion. Another 2000 years passed when human discovered that these two wonders of nature, magnetism and electricity are actually linked together like the two sides of the same coin. Since then, in the early 19th century great huge achievements were made in antennas and propagation by scientists such as Hans Christen Oersted, Heinrich Hertz, Alexander Popov and Marconi. Since then, antennas have found their enormous applications in military, medical and industrial arenas. In the endless world of antennas, we have picked up leaky wave antennas to further investigate their interesting properties and worked on at least 2 applications of such propagation systems in the medical field as well as in automotive field such as road safety. In our research, we have designed one-dimensional and two-dimensional leaky wave antennas to apply the main beam to the cancerous tissue by using the beam scanning property of these antennas. We could shift the main beam to another location in the tissue. Two-dimensional leaky wave antennas provide more beam flexibility in terms of beam geometry and beam displacement which will be discussed in the corresponding chapters.

Improving road safety with equipping vehicles with sensing systems such as frequency modulated continuous wave (FMCW) automotive radar systems is one of the most interesting topics in radar engineering. Surely, the main factor that could influence the mass production of cheap radar systems for automobiles is influenced by what antenna system is designed for that radar system. In this dissertation, we have proposed an FMCW radar system using a cheap antenna solution. The proposed antenna system is comb-line leaky wave antenna. The performance of the proposed radar system has been evaluated using range-Doppler graphs and we have also discussed a common problem in multi-target FMCW radar systems which is the issue of the ghost targets.

1 Introduction

In 1865 Maxwell derived the 4 golden equations for propagation of the electromagnetic waves. He successfully proved that varying electric field could generate varying magnetic field or vice versa. In 1888 a German physicist Heinrich Hertz made the first antennas to prove the existence of the electromagnetic waves. It is interesting that Heinrich Hertz once said that "I do not think the wireless waves I have discovered will have any practical applications". But today as we see, we are surrounded by electromagnetic waves and many applications regarding them. We could consider a considerable range of devices from daily used devices such as cell phones, tablets or microwave ovens up to the satellites that orbit the earth to provide GPS coverage, weather detection radars up to biomedical devices that are at the service of medical doctors to do diagnosis in different regions of human body such as doing chest X-rays.

The structure that is able to send and receive the electromagnetic waves is called antenna. The Britannica encyclopedia says "Antenna, also called aerial, is a component of radio, television and radar systems that directs incoming and outgoing radio waves". Since the development of the first antennas by Heinrich Hertz many more antennas have been invented which have influenced almost every aspect of our lives. We are now ready to review the basic antenna parameters.

1.1 Basic Antenna Parameters

Figure 1-1 shows the components of an antenna system including a feed, transmission line and the antenna device. From the point of view of the transmission line, antenna appears as a circuit with 2 terminals that has impedance Z with a radiation resistance that we name R_r [1].

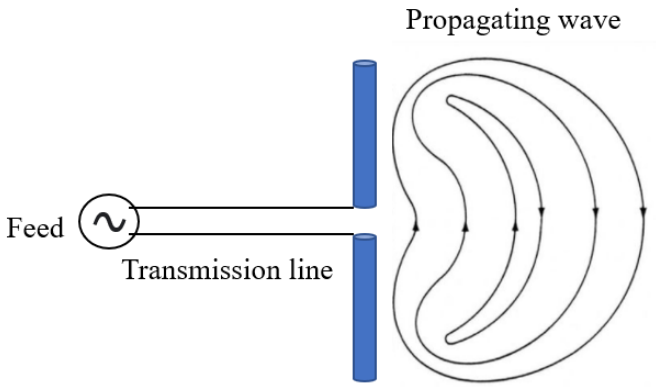

Figure 1.1. Dipole antenna propagating into free-space.

1.1.1 Antenna Pattern

We could consider a field pattern at any distance from antenna in direction φ and θ. The propagation pattern of a given antenna has a main beam and some sidelobes or back-lobes that are usually unwanted should be minimized to maximize the electromagnetic energy in the main beam.

1.1.2 Radiation Intensity

The radiation intensity is defined as the ratio of the power propagated from antenna per unit solid angle and could be expressed as ($Watts/deg^2$).

1.1.3 Directivity

The antenna directivity D is defined as the maximum radiation intensity to the average radiation intensity as defined in equation 1-1.

$$D = \frac{U(\theta, \varphi)_{max}}{U_{average}} \tag{1-1}$$

Given the efficiency factor of antenna is k (between 0 and 1), the antenna gain is defined as equation 1-2.

$$G = k.D \tag{1-2}$$

The efficiency is affected by ohmic losses inside the antenna. Clearly, more ohmic losses would not allow a considerable amount of energy to propagate from antenna but would rather heat up the antenna structure.

1.1.4 Return Loss

Return loss is actually a parameter which indicates what proportion of the input energy is reflected back to the input port and what proportion of the energy radiates. In other words, an antenna that is designed to work in a certain frequency must have the lowest return loss at that frequency which shows that the antenna has a good resonance and also impedance matching at that specific frequency. Return loss is expressed in dB scale.

1.2 Antenna Types

There is really a countless number of antennas that are interesting to study. Many textbooks or scientific papers have categorized antenna types e.g. [2] and it is still valuable to have an overview of at least the main categories of antennas that is shown on figure 1-2.

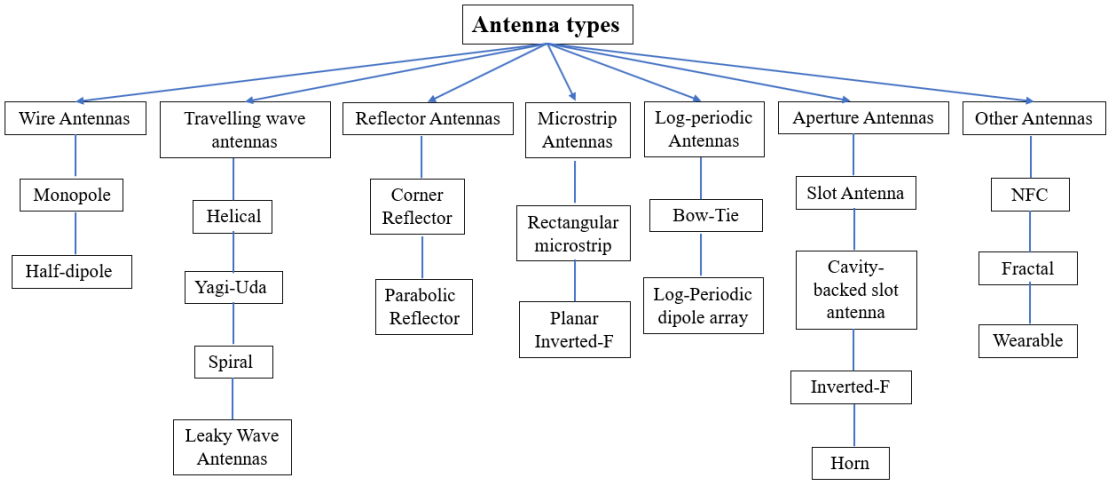

Figure 1.2. Dipole antenna propagating into free-space.

In our research, we have focused on leaky wave antennas which are in the subcategory of the travelling wave antennas according to figure 1-2. In the following section, we will explain the leaky wave antennas, theory of operation and their applications.

1.3 Leaky Wave Antennas

Leaky wave antennas (LWAs) are originated from waveguide structures and they radiate by continuous leakage of their energy into the free-space. The radiation happens by use of a fast travelling wave mode with phase velocity larger than the speed of light. The field of a given electromagnetic wave travelling along a structure can be expressed as equation (1-3).

$$\psi(\mathrm{r}) = \psi_0(\rho)e^{-jk_z z} \tag{1-3}$$

In which, z is the direction of the wave propagation and $\rho = x\hat{\imath} + y\hat{\jmath}$ expresses the transverse coordinates. The antenna structure has some apertures that could have different forms such as continuous, discontinuous or periodic. The complex wave number k_z is considered as stated in equation (1-4).

$$k_z = \beta - j\alpha \tag{1-4}$$

And the complex wavenumber vector is $k = k_\rho + jk_z\hat{z}$. In which, β is the propagation constant and α is the leakage or attenuation constant and thus by substituting the mentioned wavenumber vector in equation (1-3) we can derive equation 1-5.

$$\psi = \psi_0 e^{-j(k_\rho \rho + \beta z)} e^{-\alpha z} \tag{1-5}$$

And we can derive equation 1-6.

$$k_\rho = \sqrt{k_0^2 - k_z^2} \tag{1-6}$$

We previously mentioned that the fast wave mode causes the radiation in leaky wave antenna. The reason is that for a fast wave $v_p > c$ and that results in k_ρ being a real number which means antenna propagation into the free-space becomes possible. The angle of the antenna's main beam is defined by equation 1-7.

$$\sin(\theta_m) = \frac{\beta(f)}{k_0} \tag{1-7}$$

As we can see on equation (1-7), the propagation constant β is a function of frequency. In other words, changing the excitation frequency of a leaky wave antenna would lead to the change of beam scan angle. There are several motivations why we picked the topic of leaky wave antennas for our research. First, the property of beam scanning in leaky wave antennas that makes them appealing for any application that requires sudden displacement of antenna beam such as beam control for treatment of tumors in body where it is necessary to focus a beam of electromagnetic wave to increase the temperature of malicious cells and destroy them or in radar industry a road safety solution. The other reason is that leaky wave antennas do not need any complex feeding networks and they could be easily fed by a waveguide port as well as they are wideband antennas that show a good impedance matching for a considerable frequency range.

1.3.1 Categories of Leaky Wave Antennas

Leaky wave antennas are of three types, uniform, periodic and quasi-uniform. In addition to that they could be one-dimensional (1D) or two-dimensional (2D). In uniform structure there is no change in the transverse cross-section of the antenna structure and the cross section keeps the geometrical uniformity along the propagation axis. There is an example of a uniform LWA in Figure 1-3 which shows a leaky wave antenna that has originated from a rectangular waveguide which on one side has a baffle with a narrow radiating slit. It was first invented by Menzel [3] and the corresponding mathematics was explained by Oliner [4].

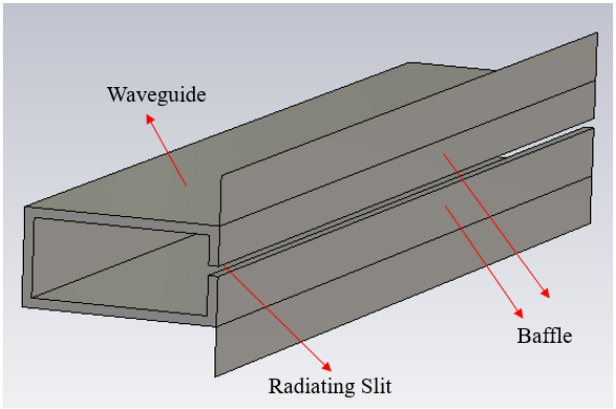

Figure 1.3. One-dimensional uniform leaky wave antenna with slit.

The second type of leaky wave antenna is periodic type in which there is a repetition of some features such as slots, stubs, permittivity or permeability along the radiation axis. Back in the 50s, Hyneman described the periodicity of slotted waveguide structures [5] using Bloch-Floquet theory [6]. Based on this theory, waveguide structures that have periodic features, such as periodic slots, are able to generate a countless number of space harmonics as expressed by equation 1-8. The parameter p is the periodicity value and n is the mode number while $\beta_0(\omega)$ is the fundamental propagation constant.

$$\beta_n(\omega) = \beta_0(\omega) + \frac{2\pi n}{p} \tag{1-8}$$

In leaky wave antennas we usually consider the harmonic $n = -1$ as the fast wave mode used for propagation. This consideration makes a design condition in LWAs which requires the period $p < \lambda_g/2$[7]. Applying this design condition would tailor the grating lobes to some extent and allows the antenna to have most of the energy focused in the main beam. In figure 1-4, we can see 2 examples of the periodic leaky wave antennas.

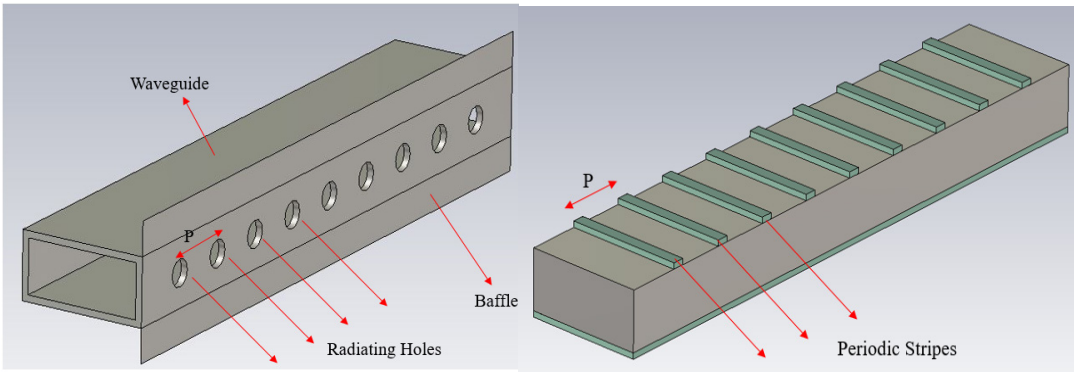

(a) (b)

Figure 1.4. Examples of periodic leaky wave antennas. (a) Leaky wave antenna with periodic holes (b) Leaky wave antenna with periodic stripes.

The third type of leaky wave antennas is quasi-uniform type. These types of LWAs are quite similar to the periodic LWAs in terms of geometry. Under the periodic structures, we mentioned that we consider the period of the structure smaller than half of the guide

wavelength. In quasi-uniform structures $p \ll \lambda_g$. In this respect, the main space harmonic $n = 0$ is actually the fast wave mode and does the main radiation from the antenna.

1.3.2 Propagation in Periodic Leaky Wave Antennas

The modal field of the periodic LWAs can be written as equation 1-9.

$$E(x,y,z) = \sum_{n=-\infty}^{+\infty} F(x,y)e^{-jk_n z} \tag{1-9}$$

In which,

$$k_n = k_0 + \frac{2\pi n}{p} \tag{1-10}$$

In figure 1-5, we can see a periodic leaky wave antenna that is composed of a microstrip line connected to 32 stubs and 2 quarter-waveform transformers connected to both left and right hand-side ports. This antenna is called comb-line leaky wave antenna and in chapter IV it will be further discussed.

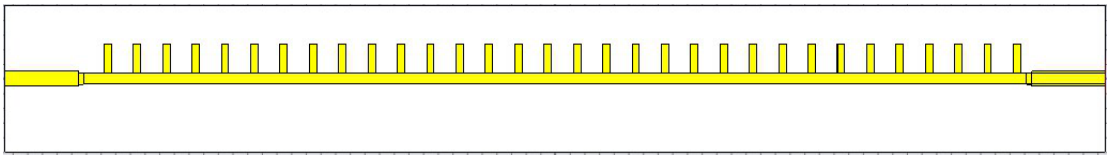

Figure 1.5. Comb-line leaky wave antenna.

In periodic leaky wave antennas for some modes $k_n = 0$. We can explain this phenomenon from the circuits point of view and that is at a given frequency all the periodic subs short out and the equivalent circuit of the antenna at this critical frequency becomes symmetrical where all the cells show impedance Z_0 and the antenna impedance from the view of the excitation ports turn into zero or very small thus the radiation resistance would be very small too. This impedance is called Bloch impedance in the literature. Then standing waves will form which of course will not propagate from the antenna.

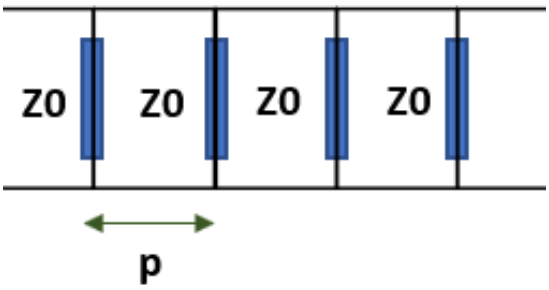

Figure 1.6. Circuit equivalent of a periodically stubbed leaky wave antenna.

There are different methods proposed to introduce asymmetry in the antenna structure and avoid the broadside issue. For example, in [8] the authors have introduced matching stubs in each cell of the LWA such that the Bloch impedance will not drop to zero at broadside. In [9], introducing inductive posts on both sides of periodic slots could compensate for the mismatched impedance and enhance the broadside propagation.

1.3.3 Application of leaky wave antennas in hyperthermia

Tumor is an abnormal growth of tissue caused by malicious cells in the body. Tumors could be either benign or malignant. Medical doctors have always been in search of tumor treatment methods that would result in minimal side effects and more rapid recovery. Invasive treatments such as surgery could carry more risks than non-invasive methods such as propagation therapy. There would also be a higher chance of rapid recovery by using non-invasive methods. The Beam scanning capability of leaky wave antennas makes them good candidates for such task. Already in the corresponding literature there are several proposed antennae designs for hyperthermia treatment in different regions of the patient's body. In [10], the proposed system is a dual band pyramidal horn antenna for breast hyperthermia treatment. The feeding network for this antenna is an array of ten directors of Yagi antennas that are capable of applying power of 2 Watts for 10 minutes. The authors have observed a temperature rise of about 4℃ in the test tissue. In [11], a compact microstrip antenna has been designed as hyperthermia applicator. The authors have used a head phantom from CST library to mimic the real human's head and have put an array of

4 antennas around the head while a small sphere was considered as tumor to be heated up by the system. The current literature agrees on the fact that a temperature range such as 41℃ to 45 ℃ is appropriate for destroying the malicious cells and basically mild temperatures are recommended to avoid damaging the healthy cells that surround the cancerous cells. In our published work [12] we have shown that a substrate integrated slotted waveguide leaky wave antenna could be used for hyperthermia treatment in frequency range of 13.5 GHz to 15.2 GHz. The state-of-the-art hyperthermia systems rather use antenna arrays that usually need complex feed networks such as the SIGMA-Eye applicator that uses 12 antennas [13]. Our proposed design is simple in geometry and cheap to manufacture and does not have the problem of having complicated feeding networks. To the best of our knowledge, using leaky wave antennas for hyperthermia is a novel research area yet to be explored.

1.3.4 Application of leaky wave antennas in FMCW Radars

Each year many people lose their lives in road accidents either as drivers or pedestrians. That is why, it is absolutely necessary to equip more and more cars with radar systems to diminish road accidents and increase safety both for drivers and pedestrians. Radar solutions are economical, usually simple in structure and robust in different scenarios such as rainy weather in which LIDAR or camera might face target detection challenges. There are 2 types of radars: 1) pulse radars 2) frequency modulated continuous wave radars (FMCW). Pulse radars tend to send a very short time signal with a considerable amount of transmit power and then wait for the echoes reflected back from the target but the FMCW radars continuously send signals and measure the velocity and the range of the target using frequency difference between the sent and received signals. For the sake of the high-power consumption, they might not be the best options for the automotive industry. While continuous wave radars are very power efficient, have simple solid-state transmitters and also good range resolution [14-16]. We must consider that low power consumption in FMCW radars leads to more limited target ranges compared to pulse radars since the radar transmit power has direct impact on the radar range according to equation 1-11 in which P_{Tx} is the transmitted power, G_{Tx} is the transmit antenna gain, G_{Rx} is the receive antenna

gain, λ is the wavelength of the radar signal, σ is the radar cross section (RCS) and S_{min} is the minimum detectable signal threshold. We can see that for example to double the range, we need to increase the transmit power by 16 times. However, for automotive applications it is enough for drivers to detect targets within a few hundred meters in front of their cars which means detecting a limited range would not be problem.

$$R = \left[\frac{P_{Tx} G_{Tx} G_{Rx} \lambda^2 \sigma}{S_{min} (4\pi)^3}\right]^{1/4} \quad (1\text{-}11)$$

The operation theory of the FMCW automotive radars and the corresponding equations are explained in chapter IV and here we just point out to the highlights. There is relatively a considerable volume of published work on FMCW radars for automotive and road safety applications but a few of them have focused on leaky wave antennas as efficient and cheap solutions compared to complex beamforming networks or antenna arrays. The focus of any radar research could be in improving the performance of the RF circuitry, signal processing algorithms or the development of antenna systems to reach higher radar resolutions both in the range and the velocity. For example, in [17], the authors have proposed a radar system that uses a substrate integrated waveguide leaky wave antenna for direction of arrival estimation (DOA) in multiple-target scenario. In [18], a unique radar chirp is introduced which could lead to less ambiguity in target detection. In multi-target scenarios, radar systems usually face with ghost targets which are radar detections that originate from anything other than the actual targets. We will discuss the ghost target issue in chapter IV.

The following chapters are as follows, in chapter II, we will discuss a proposed 1D slotted leaky wave antenna for hyperthermia treatment, in chapter III we will introduce several 2D leaky wave antennas and will discuss the specific absorption ratio (SAR) as an evaluation tool for the acceptable ranges of EM absorption by human body tissues. In chapter IV, we will introduce an FMCW automotive radar system with comb-line leaky wave antenna as beamforming system and the discussion of performance versus the state-of-the-art beamformers. In chapter V, we will conclude this thesis by summary of our research and the future work.

1.4 References

[1] John D. Kraus, Antennas. McGraw-Hill, 1950.

[2] Johnson, Maryson, et al. "Survey on Antennas and their Types."

[3] W. Menzel, "A new traveling-wave antenna in microstrip," Archiv fur Elek-tronik und Ubertragungstechnik (AEU), vol. 33, no. 4, pp. 137–140, April 1979.

[4] A. A. Oliner, "Leakage from higher modes on microstrip line with applications to antennas," Radio Science, vol. 22, no. 6, pp. 907–912, Nov. 1987.

[5] Hyneman, R. "Closely-spaced transverse slots in rectangular waveguide." IRE Transactions on Antennas and Propagation 7.4 (1959): 335-342.

[6] Brillouin, Leon. Wave propagation in periodic structures: electric filters and crystal lattices. Vol. 2. Dover publications, 1953.

[7] W. W. Hansen, "Radiating electromagnetic waveguide," Patent, 1940, U.S. Patent No. 2.402.622.

[8] Paulotto, Simone, et al. " A novel technique for open-stopband suppression in 1-D periodic printed leaky-wave antennas. " IEEE Transactions on Antennas and Propagation 57.7 (2009): 1894-1906

[9] Ranjan, Ratnesh, and Jayanta Ghosh. "An enhanced beam scanning leaky-wave antenna with suppressed open-stop band." 2018 3rd International Conference on Microwave and Photonics (ICMAP). IEEE, 2018.

[10] Tayel, Mazhar Basyouni, Tamer Gaber Abouelnaga, and Azza Elnagar. "Dielectric loaded Yagi fed dual band pyramidal horn antenna for breast hyperthermia treatment." 2018 5th International Conference on Electrical and Electronic Engineering (ICEEE). IEEE, 2018.

[11] Isik, Omer, et al. "Development of a hyperthermia applicator with compact microstrip antennas." Proceedings of the 2012 IEEE International Symposium on Antennas and Propagation. IEEE, 2012.

[12] Sarabi, Masoud, and Warren Perger. "A Novel Leaky Wave Antenna for Hyperthermia." 2019 IEEE Texas Symposium on Wireless and Microwave Circuits and Systems (WMCS). IEEE, 2019.

[13] Gellermann, Johanna, et al. "A practical approach to thermography in a hyperthermia/magnetic resonance hybrid system: Validation in a heterogeneous phantom." International Journal of Radiation Oncology* Biology* Physics 61.1 (2005): 267-277.

[14] C. Li, Y. Xiao, and J. Lin, “Experiment and spectral analysis of a low-power K a-band heartbeat detector measuring from four sides of a human body,” IEEE Transactions on Microwave Theory and Techniques, vol. 54, no. 12, pp. 4464–4471, 2006.

[15] M. Wakayama, H. Ezaki, I. Arai, and T. Miwa, “Non-contact measurement of heart rate using FM-CW radar,” IEICE Technical Report SANE2005-3, 2005.

[16] I. Arai, “Life-detection radar for rescue purpose,” IEICE Technical Report SANE99-100,2000

[17] Steeg, Matthias, Asmaa Al Assad, and Andreas Stöhr. "Simultaneous DoA estimation and ranging of multiple objects using an FMCW radar with 60 GHz leaky-wave antennas." 2018 43rd International Conference on Infrared, Millimeter, and Terahertz Waves (IRMMW-THz). IEEE, 2018.

[18] Lin, Jau-Jr, et al. "Design of an FMCW radar baseband signal processing system for automotive application. " SpringerPlus 5.1 (2016): 1-16

2 A Novel Leaky Wave Antenna for Hyperthermia

2.1 Introduction

Non-invasive methods for removal or elimination of carcinogenic tissues in human body, have priority over invasive medical methods such as surgery. Surgeries always carry risks and also cause a higher potential of disease relapse, while non-invasive methods have less risks, lead to more rapid recovery and could reduce the recurrence of symptoms. Therefore, they could be more successful in medical treatments. Amongst non-invasive methods, one can mention hyperthermia, which is defined as heating up a body tissue with a medical device to reach the above-normal temperatures in order to destroy or at least linger the growth of the abnormal cells such as the carcinogenic ones in different tissues of the human body. Hyperthermia mechanism can be introduced by SIW leaky wave antenna that has a cheap and simple manufacturing process, and as is the case for these antennas, they could successfully do beam scanning with frequency change. The proposed antenna has 12 rectangular slots [1] and 88 copper via. Decades back, this antenna and its properties were not much known, due to the complicated math used to describe the wave propagation by this antenna [2]. But today, our knowledge of these travelling wave antennas is more comprehensive than before thanks to the powerful software packages such as CST Microwave Studio, HFSS, FEKO and other simulation tools.

For instance, we know the necessity of having series of rectangular slots to introduce periodicity that originates from the Floquet theorem or the essentiality of having copper via in the antenna to render less leakage of the EM wave through the side walls, having better VSWR characteristics as well as better connection of surface currents' distribution on the metallic planes of the antenna [2]. In this respect, we introduce a novel leaky wave antenna, whose dimensions are partly inspired by [3]. This antenna is from the family of the substrate integrated waveguide leaky wave antennas, which originate from a simple parallel-plate waveguide and develop into a leaky wave antenna by introducing slots and via. To approach optimal design parameters, we studied the change of many design parameters such as feed-line, slot length, via spacing, etc. and put them under test in the simulation environment. We know that substrate permittivity, via diameter, slot length and

width, substrate thickness and feeding port's dimensions, the excitation pulse and thickness of ground plane can each be, a key parameter that might strongly affect the antenna's propagation characteristics such as radiation pattern, Side Lobe Level (SLL), efficiency, directivity of the main beam and its proximity to the broadside or end-fire directions. Thus, many simulations were done and the best achieved results are presented in this paper.
In section 2, we will introduce the antenna topology along with design parameters and discuss the simulations and in section 3. In the last section of this paper, we will discuss the conclusions. For all simulations, CST Microwave Studio as well as MATLAB were used.

2.2 Transverse Slotted Leaky Wave Antenna

The antenna designed for hyperthermia should be used in close proximity to the human body, for example 3mm to 4mm above antenna, to be able to take advantage of the near field of the antenna. The antenna is composed of an extremely thin ground plane $h_g = mm$ and a substrate of RT6010 with thickness $hsubstrate$ and on top of that a superstrate, whose dimensions are included in table 2-2. The feedline is actually about 3mm longer than the $\lambda/4$ length and this optimal length was achieved during tuning process of antenna in the design stage. This length increase could optimize the VSWR and return loss characteristics considerably. Figure 2-1 shows the top view of the proposed antenna. There are 12 rectangular slots to cut the current paths and excite leaky modes. A row of 44 copper via on each side of the transverse slots connects the ground plane and the superstrate. Considering an appropriate length and width for a slot is also a delicate and sensitive work, since these design parameters could directly affect the excitation of modes or change the radiation pattern. We can, for instance, end up with huge sidelobes, if the slot width is not small enough. Based on the literature by Preez et al. [4], to have a single beam radiation, we would need the substrate permittivity to hold in equation 2-1, where, Sp is the periodic distance between slots and a indicates the greater dimension of the waveguide. Thus, $\in_r =$ 10 was considered.

$$\in_r > 9 + \left(\frac{S_p}{a}\right)^2 \qquad (12\text{-}1)$$

To avoid having grating lobes, we would need the slots spacing not to be bigger than $\frac{\lambda}{2}$ [5].

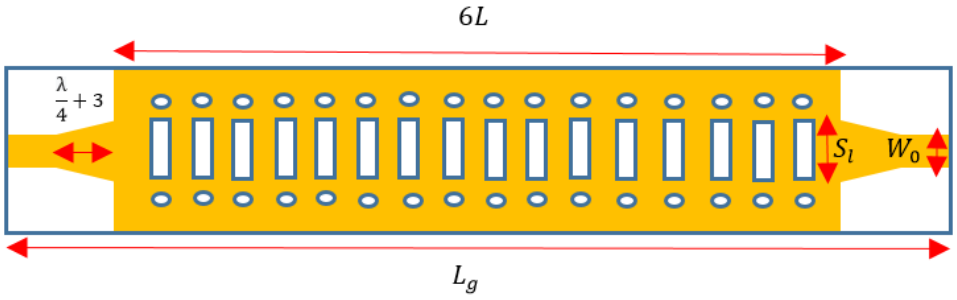

Figure 2.1. Realization of leaky wave antenna in CST Studio.

Table 2.1. Dimensions of the proposed leaky wave antenna.

Parameter	**Dimensions (mm)**	**Description**
$L_g \times W_g$	$154 * 21.52$	Ground plane
$L_s \times W_s$	$154 * 21.52$	Substrate
L_{slot}	7	Slot length
W_{slot}	2	Slot width
d_{via}	1.1	Via diameter
d_{vv}	18	Transverse via-to-via distance
d_{hh}	3	Horizontal via-to-via distance
$h_{substrate}$	1.75	Substrate thickness

2.3 Simulation Results

In this section, we are going to investigate the details and results of our simulations, using CST Studio and MATLAB. Simulations were implemented by a 4GB RAM computer. A waveguide port for pulse excitation was defined for the antenna, and the frequency range was from 13.8 GHz to 15.2 GHz. Regarding the topology of the excitation pulse, it is noteworthy to mention that many different pulses such as Gaussian, trapezoid, rectangular and triangular, were tested to understand which of the pulses could result in better return

loss and higher directivity and possibly higher temperature rise. We considered two factors for each test pulse, amplitude and pulse width. After trying different pulses, we found the desired one to be trapezoidal and with pulse width of 325 seconds. The three pulses used for excitation are shown in Figure 2-2. The EM solver chosen for our simulation was the frequency solver based on the antenna structure or the range of frequency. The choice of EM solver also depends on the size of the structure. Usually, when the biggest dimension of the antenna is smaller than 10 λ, then using the frequency solver would be the best option [11]. Since for example compared to the time domain solver, frequency solver could be less time-consuming. Besides, usually the frequency solver is preferred over the time domain solver when we face single frequency or limited frequency range applications. For example, for our antenna $f_H - f_L = 1.4$ GHz (difference between higher and lower frequency) and the choice of the frequency solver is then a rational choice. For the first part of the simulations, we have included the return loss graph shown in Figure 2-3. We can observe that for most of the frequency points, the return loss $|S11_{dB}| < -10\,dB$ proves good impedance matching at the feeding port of the leaky wave antenna, while, the minimal loss happens at approximately f = 14.2 GHz.

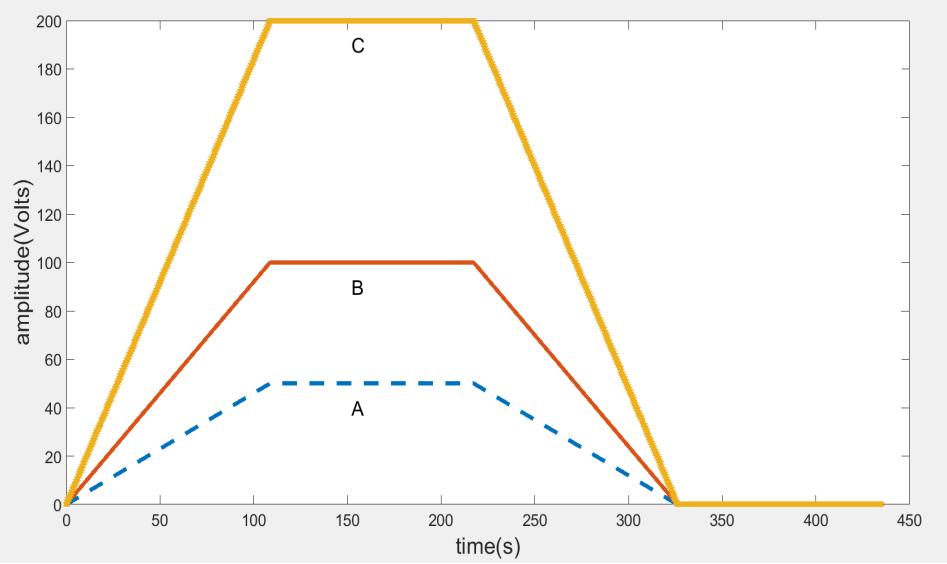

Figure 2.2. The envelopes of excitation pulses used for the proposed transverse slotted leaky wave antenna. The amplitudes are A=50v, B=100v, C=200v.

The thermal simulations are done based on two types of boundary conditions (BCs), the isothermal BC and the adiabatic BC. In both cases, along X and Y axes, boundary conditions are isothermal, while across Z axis they could be either isothermal or adiabatic.

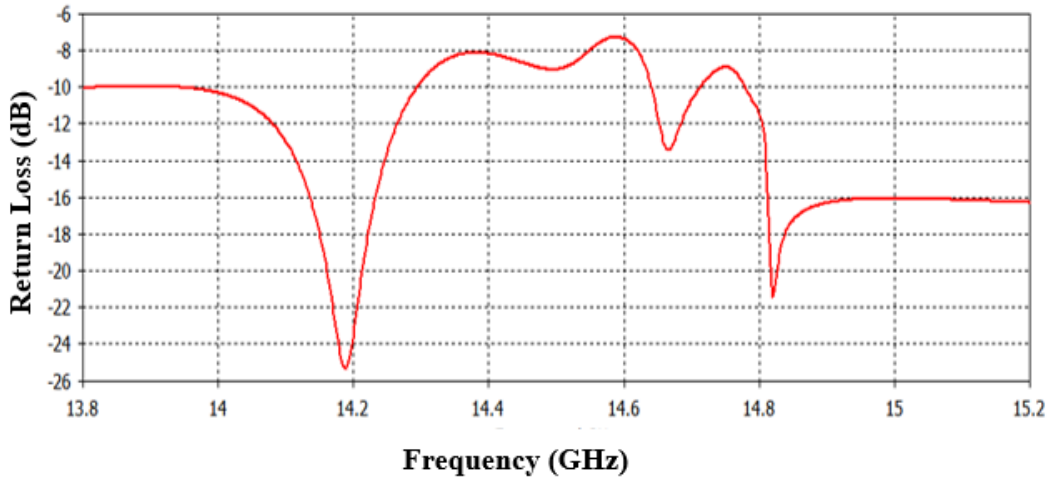

Figure 2.3. The return loss graph of the proposed transverse slotted leaky wave antenna

We know from thermodynamics [10] that in the isothermal process the temperature is considered as constant and the Ideal Gas Law stated in equation 2-2 results in reciprocity of pressure (P) and Volume (V).

$$PV = nRT \tag{2-2}$$

In Figure 2-4, we can see 3 diagrams for 50v, 100v and 200v each describing the isothermal thermal response of the proposed antenna to different excitation frequencies for the given trapezoidal pulses. By comparing these three, we are looking for a gradual temperature rise by frequency scanning and the most optimal and ideal graph is the blue one, corresponding to the 50v excitation pulse. That's noteworthy, since for medical applications depending on the severity of a tissue and our motivation for destroying it, we are able to switch to higher temperatures by changing the applied frequency. This expectation is fulfilled in all three given pulses but as we see regarding the pulses other than 50v, we can't necessarily say that by increasing the frequency the temperature rises. But it is more precise to mention that increasing the frequency leads to the increase or decrease of the temperature in proportion to the former frequency point. Also, from the technical point of view using

milder temperatures for a longer time is a more appropriate choice, rather than applying much higher temperatures.

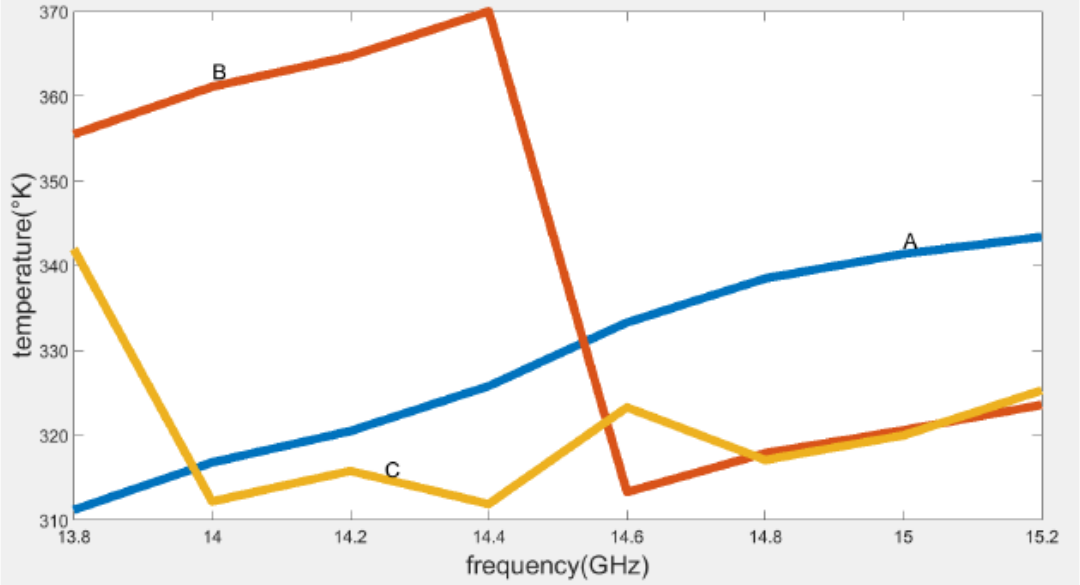

Figure 2.4. Temperature vs. frequency plots isothermal along Z. The letters A, B and C correspond to 50v, 100v and 200v pulses correspondingly.

By referring to thermal patterns for 100v and 200v pulses, we can see that temperatures, sometimes reach up to 370 °K (96 °C) for isothermal BC, thus, much higher than the peak of the 50v's thermal response, which is at around 343 °K (69.85 °C). Next, in Figure 2-5 we can see the thermal simulation results for the adiabatic boundary condition along Z. From thermodynamics, we know that in adiabatic process, there is no heat transfer to or from our system, in other words, it's considered as a closed system ($dQ = 0$). Equation 2-3 states the adiabatic process.

$$PV^{\gamma} = Const. \qquad (13)$$

In which, P is pressure, V is volume and γ is the specific heat ratio. Fig. 5 proves that applying the adiabatic boundary condition could lead to higher temperature values compared to the isothermal BC. Still the most logical temperature curve for medical purposes, seems to be the one corresponding to 50 v, as was the case for isothermal

boundary condition too.

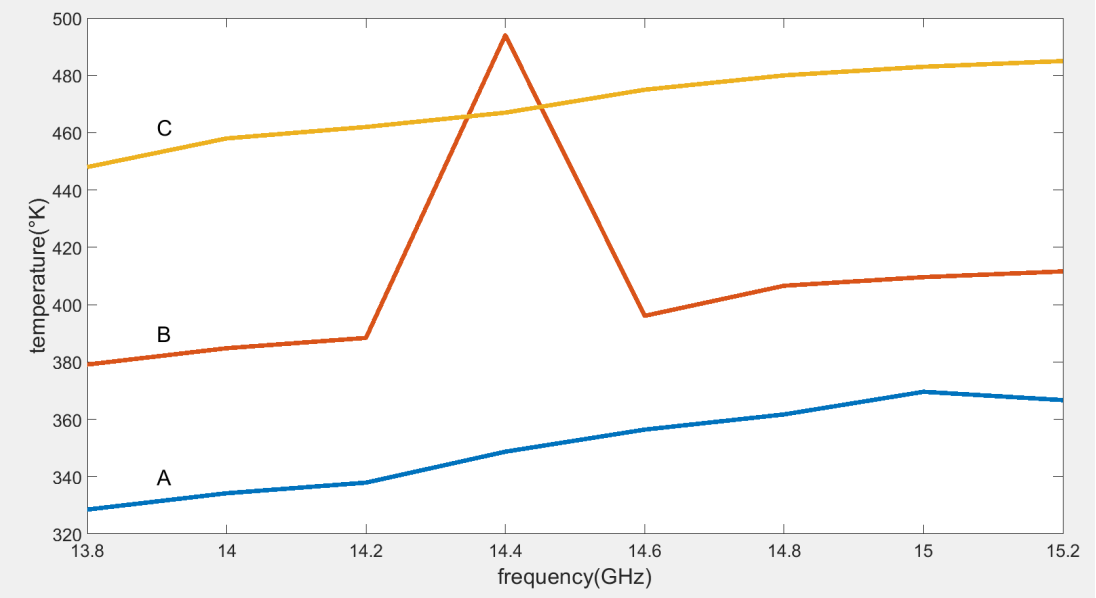

Figure 2.5. Temperature vs. frequency plots adiabatic along the Z-axis. The letters A, B and C correspond to 50v, 100v and 200v pulses correspondingly.

Then, the directivity versus frequency plots of the three mentioned pulses are shown in Figure 2-7. With a fairly good approximation, we can conclude that we have the same directivity for all three applied pulses. If we look closely, only the directivity corresponding to 50v pulse, shown in dashed line between 13.8 GHz to 14.4 GHz is different from the other two but after 14.4 GHz, all the three graphs really have good matching with each other. Frequency points have spacing of 200 MHz, starting from 13.8 GHz and ending at f = 15.2 GHz. We think that from the medical point of view it is quite useful to know, at which frequency points we have fan beams and at which frequency points we have pencil beams [6] because the shape of the beam and the matter of how sharp or how flat the beam looks can directly affect the size of the heated area.

Next, Figure 2-8 is corresponding to the total radiation efficiency graph. We observe that the efficiency has an increasing trend in 13.8 GHz to 14.2 GHz, but from 14.2 GHz to 14.6

GHz, we have a decreasing trend, while once again, the efficiency increases after 14.6 GHz, with the maximum efficiency of -4 dB occurring at f = 14.2 GHz. Meanwhile; specific absorption ratio (SAR) is an analysis tool that could further prove the capability of the proposed design for hyperthermia. Figure 2-6 illustrates the SAR pattern of the heated area and the size of it, using 50V pulse at f = 14.4 GHz which was done in CST.

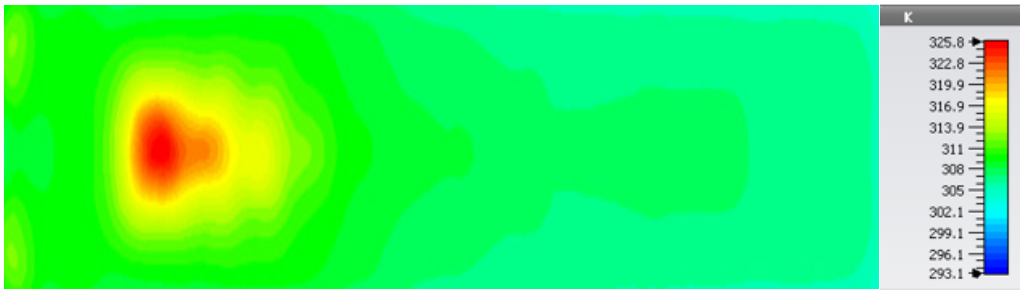

Figure 2.6. Specific absorption ratio (SAR) analysis for 50V pulse at f = 14.4 GHz

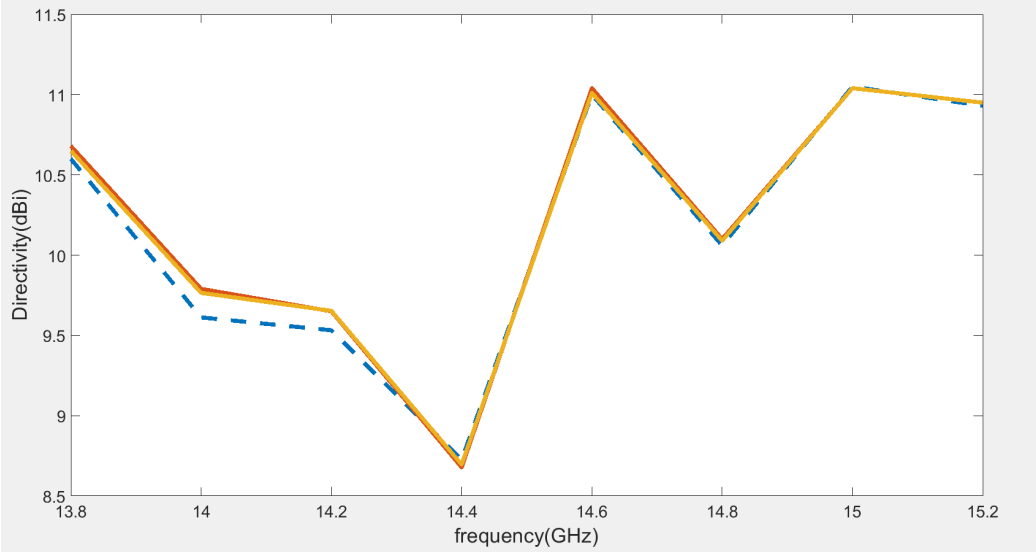

Figure 2.7. Directivity vs. frequency plot for 50v, 100v and 200v pulses.

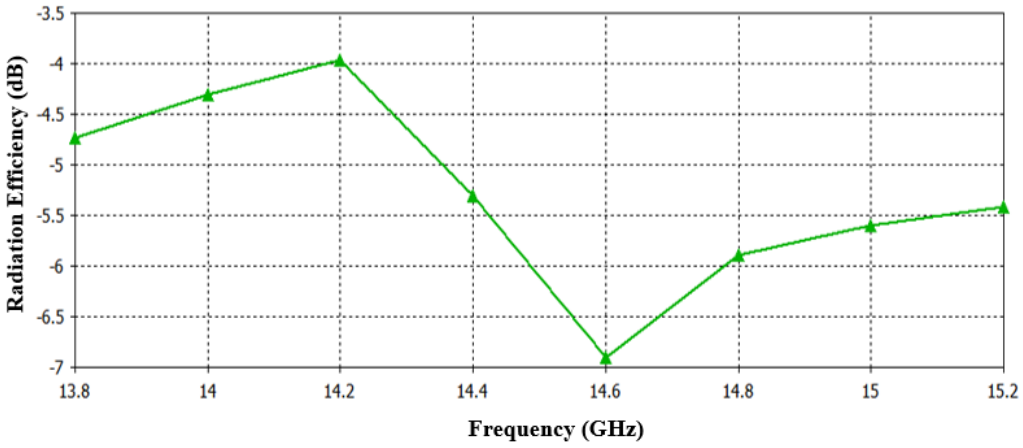

Figure 2.8. Total radiation efficiency vs. frequency

Figure 2-9 shows the propagation pattern of our proposed antenna simulated in CST, at a sample frequency of f = 13.8 GHz. As is the case, for leaky wave antennas of this type, by gradually increasing the frequency, we can scan from near broadside region to near end-fire. There are some techniques for elimination of open stop-band problem, for avoiding the Bloch impedance from becoming zero near broadside [7].

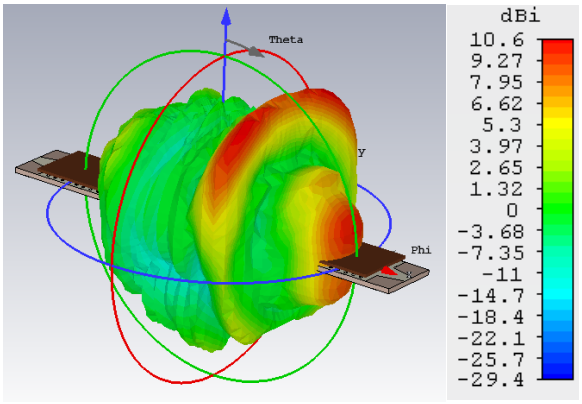

(a)

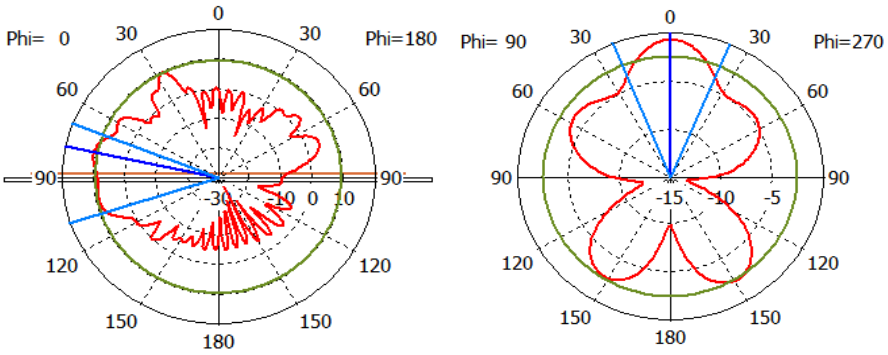

(b) **(c)**

Figure 2.9. (a) Three-dimensional propagation pattern of the proposed antenna at f=13.8 GHz (b) Polar pattern at E-plane (c) Polar pattern at H-plane

2.3 Conclusion

In this paper, a slotted substrate integrated waveguide leaky wave antenna for operation in 13.8 GHz to 15.2 GHz was proposed and for the very first time this type of antenna was considered for hyperthermia which is one of the possible medical applications as a non-invasive method for cancerous tissue elimination in human body. After introducing the antenna structure and its geometry, we presented the results of EM simulations using frequency solver of CST software and finally studied the thermal patterns on the test tissue,

in our case liver, situated in the near field of this antenna. Thermal simulations were done for two different boundary conditions, isothermal and adiabatic. The question of how precisely we could create the lab conditions for the adiabatic BC can be best answered in future studies after fabricating this antenna and testing it in a thermally controlled environment, to be able to approximate a thermally closed system as adiabatic mechanism. For now, the results seem to be promising, and we think there is more room for further research on this topic. However, many other simulations are yet to be done with different types of leaky wave antennas, different feeds, slot dimensions or substrates to be able to delve further into this area.

2.4 References

[1] Xu, Feng, and Ke Wu. "Guided-wave and leakage characteristics of substrate integrated waveguide." IEEE Transactions on microwave theory and techniques 53.1 (2005): 66-73.

[2] Hyneman, R. "Closely-spaced transverse slots in rectangular waveguide." IRE Transactions on Antennas and Propagation7.4 (1959): 335-342.

[3] Shokry, M. A., A. M. Allam, and Raed M. Shubair. "Design of a periodic substrate-integrated-waveguide leaky-wave antenna." Antennas and Propagation & USNC/URSI National Radio Science Meeting, 2017.

[4] Du Preez, Jaco, and Saurabh Sinha. Millimeter-wave antennas: configurations and applications. Springer, 2016.

[5] Sutinjo, Adrian, Michal Okoniewski, and Ronald H. Johnston. "Radiation from fast and slow traveling waves." IEEE Antennas and Propagation Magazine 50.4 (2008).

[6] Jackson, David R., Christophe Caloz, and Tatsuo Itoh. "Leakywave antennas." Proceedings of the IEEE 100.7 (2012): 2194- 2206.

[7] Paulotto, Simone, et al. "A novel technique for open-stopband suppression in 1-D periodic printed leaky-wave antennas." IEEE Transactions on Antennas and Propagation 57.7 (2009): 1894- 1906.

3 Two-dimensional Leaky Wave Antennas for Hyperthermia

3.1 Introduction

To deal with cancerous tumors, a nonsurgical method known as hyperthermia can be applied in which the electromagnetic radiation of the near field of an antenna or applicator can be exposed to a specific region of a given tissue and heat it up such that the regions other than the cancerous ones are not affected by this radiation and thus no temperature rise should happen in the surrounding regions. Hyperthermia could have two types: 1) superficial hyperthermia (SHT) 2) deep hyperthermia (DHT). SHT is usually used for the tumors that are found in depths of about 4cm or less and DHT is of course for tumors that are in deeper regions. Usually the hyperthermia temperature range is between 40℃ and 44℃. The metabolism as well as the blood flow of the malignant cells are different from the normal cells and they are also more sensitive to heat and so they can get warmer than the normal cells when they are exposed to microwave heating systems. The core fact that initiates the idea of using hyperthermia mechanism as a treatment method is that the conductivity and the dielectric constant of the cancerous tissue are higher than ordinary cells [1]. Different antenna types and focusing methods have been proposed in the literature. The application of each antenna or applicator depends on the dimensions of a tumor, depth of the tumor and of course the intrinsic characteristics of the tissue such as conductivity. These factors could lead us towards either invasive or non-invasive methods. For superficial tumors, microstrip patch antennas can be used while for deep-seated tumors slot antennas can be used that are able to actually penetrate into a tissue since for such tumors heat needs to be transferred to the depth [4]. In [8], a microwave hyperthermia system using a coaxial-slot antenna in both single and array forms has been introduced. The single antenna was used to treat a shallow tumor in the right shoulder area of a 60-year-old patient and the array applicator was used for the treatment of a tumor in the right shoulder region of a 61-year-old patient. Another interesting literature proposes a balun-free helical antenna with two different matching systems of quarter-wave network and also a π-network. This system was tested upon a bovine liver tissue using the input power of 42W for time length of 5 to 10 minutes [9]. Another design has been introduced in our

earlier work [10] that shows a substrate integrated waveguide leaky wave antenna in higher frequency ranges other than medical frequencies. Antenna arrays are typically used to illuminate the beam on a tissue with higher focusing capability compared to single-antenna systems. For instance [2] introduces a hexagonal focused array that operates in 433MHz. In this design there is an array of patch antennas located on each side of the hexagon and the sample bio-tissue is placed at the center of this structure to be heated up. In [3] a SIGMA-Eye applicator array has been designed. The applicator system consists of three rings of dipole antennas where each ring has 4 pairs of antennas. The best performance with this applicator array has been observed when all the antennas where in phase and fed with the same power. In [4], the authors have introduced two types of antennas that both function at 2.45 GHz frequency. Usually, in order to treat malignant tumors that are in-depth, antenna arrays are used. Lower working frequencies such as 915 MHz could provide a considerable heat penetration and to avoid having superficial skin burns a water bolus is basically used that is placed between the antenna system and the tissue [5]. Some designs are introduced to have hyperthermia treatment for a specific part of the body. For example, in [6] a patch antenna design is used as a phased-array head and neck applicator. Based on [7] and [8] the most optimal configuration for head and neck hyperthermia is a circular array and in [6] the same setup is used that consists of 12 antennas. This paper is organized as follows: in section II, we are going to discuss the proposed antenna structures and evaluation of their electromagnetic performances such as propagation patterns and return loss. In section III the SAR mechanism and heating methodology will be discussed. Section IV will contain the results and discussion and the conclusion will be given in section V.

3.2 Antenna Structures and Performance

In this research we designed 3 different types of leaky wave antennas and investigated their application as hyperthermia treatment tools. We will introduce each antenna (subsections A, B and C) with the corresponding structure as well as beamforming capabilities, directivity and will finally focus on the thermal graphs (i.e. specific absorption ratio analysis). The study of the SAR graphs is a promising tool to understand which antenna could produce focused beams and which antenna could thermally affect larger areas of a

given tissue. The subject of the tissue area really depends on how big the area of the malignant cells is and that is why it is significant to have an estimate of the dimensions of the area to be treated in a given tissue and then calculate the area that each antenna can heat up in mm^2.

3.2.1 Two-dimensional mushroom-type Leaky Wave Antenna

The mushroom-type leaky wave antenna is composed of the following parts: a ground plane of a perfect electric conductor (PEC) that is $159.7mm \times 159.7mm$, a substrate of TMM 10i with $\varepsilon_r = 9.8$ and the same planar dimensions as the ground plane and height of H_s=1.7 mm. There are 47 by 48 square cells that are each connected to the ground plane by via. The ground plane has two u-shaped slots and has a microstrip line. So, this antenna is fed through the ground plane using a waveguide port. The excitation signal is a gaussian signal and the frequency range of simulation is $f = 2GHz$ to $f = 4GHz$.The FCC organization has allocated the central frequency of $f = 2.45GHz$ for medical applications which is also the focus of the simulations in this paper too. But it is also very informative to study the heat absorption or specific absorption ratio in bio-tissues e.g. in mm-range frequencies such as the study that was done in [11].

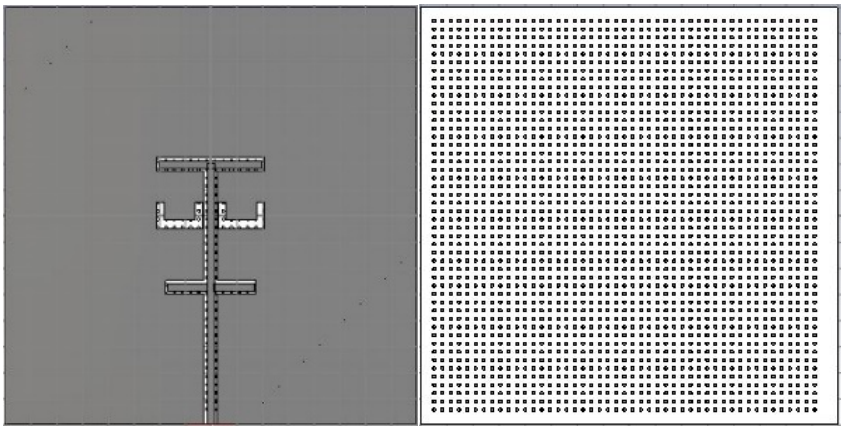

(a) (b)

Figure 3.1. (a) The structure of two-dimensional Mushroom-type leaky wave antenna(a) back side (b) front side.

Figure 3-2 illustrates the propagation pattern of this antenna at 2.45 GHz as well as the return loss graph.

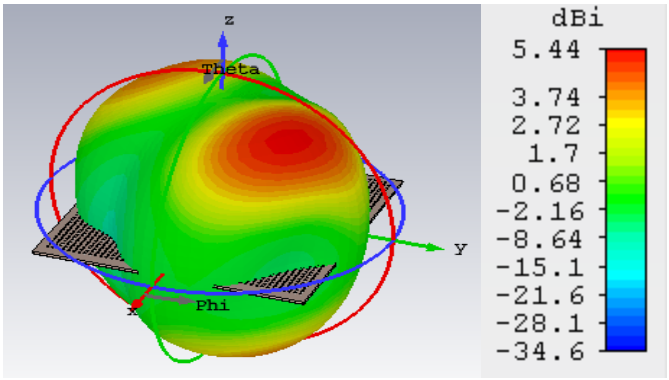

(a)

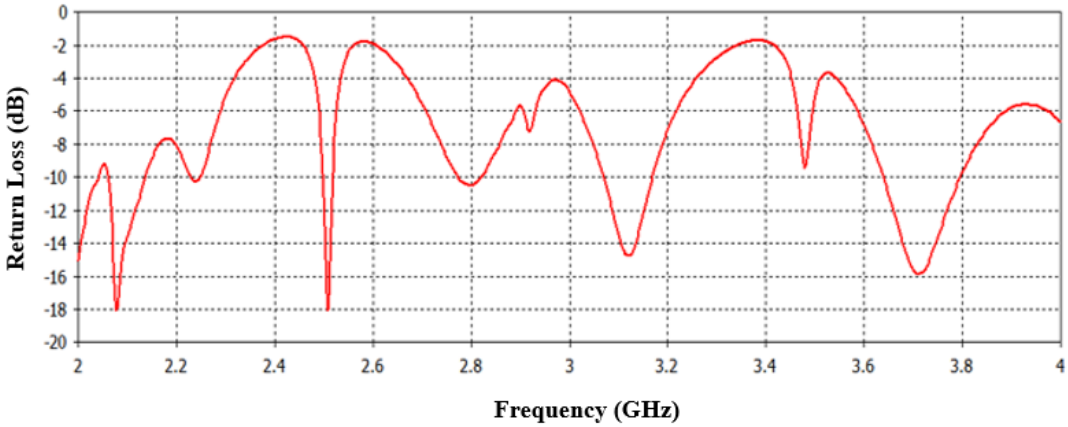

(b)

Figure 3.2. (a) Propagation pattern of mushroom-type LWA at 2.45 GHz (b) Return loss graph.

3.2.2 Two-dimensional Periodically slotted Leaky Wave Antenna

In this type of leaky wave antenna, there is a ground plane of perfect electric conductor (PEC) with dimensions of $400mm \times 400mm$ and two different substrates, Rogers RT6010 with $\varepsilon_r = 10.2$ and RO3003 with $\varepsilon_r = 3$. Each individual substrate cell is $40mm \times 40mm$ and the whole substrate consists of 100 cells. The authors think that by using 2 different columns of substrates, one could achieve certain interesting propagation properties such as having more beam flexibility which could be of high interest in biomedical applications that need beam focusing. The superstrate or top plate is PEC and

has 39 slots in x direction and 23 slots in y direction. The slots are responsible for the leakage mechanism in this leaky wave antenna. There are 2 tapered feeding lines connected to both sides of the superstrate. The tapers are for having better impedance matching properties and thus it could lead to lower return loss values for this antenna structure.

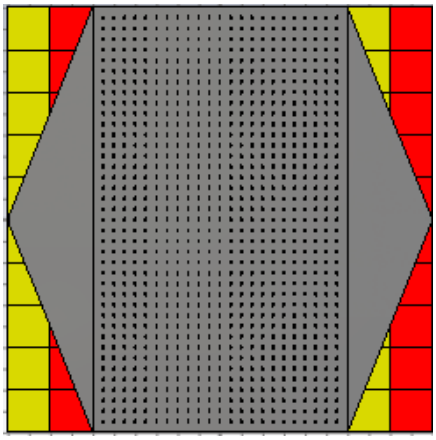

Figure 3.3. (a) The structure of two-dimensional periodically slotted leaky wave antenna.

Figure 3-4 illustrates the propagation pattern of this antenna at 2.45 GHz as well as the return loss graph.

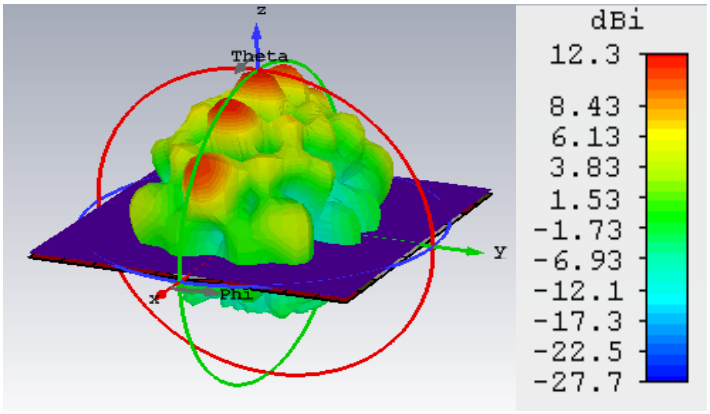

(a)

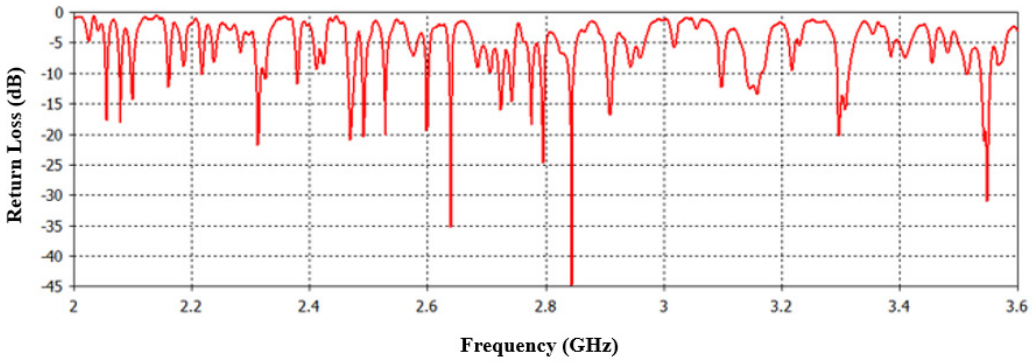

(b)

Figure 3.4. (a) Propagation pattern of 2D periodically LWA at 2.45 GHz (b) Return loss graph.

3.2.3 Belt-shaped leaky wave antenna

In this section we would like to introduce the belt-shaped or conformal leaky wave antenna (LWA) for the first time. To the best knowledge of the authors, there is no similar work to this one at the time that this paper is being written. In the belt-shaped LWA, we actually have a one-dimensional slotted leaky wave antenna with a tapered microstrip feeding mechanism as shown on Figure 3-5. In this structure, the main motivation is to have a conformal antenna that could go around the head, neck, breast, etc. or wherever there is a malignant tissue to be dealt with using hyperthermia method. So, in the simulation

environment the tissue was placed at the center of the cylinder and the thermal distribution patterns of the given tissue were studied. The substrate is TMM10 with permittivity value of $\varepsilon_r = 9.2$. In a given leaky wave antenna, especially one-dimensional type, we usually consider the $n = -1$ as a fast mode, i.e. $V_{phase} > c$ (c=speed of light) and plugging it into the Floquet equation 3-1:

$$\beta_n = \beta_0 + \frac{2\pi n}{p} \tag{3-1}$$

Which for $n = -1$, will give the following inequality (2):

$$\left|\beta_0 - \frac{2\pi}{p}\right| < |\beta_0| \tag{3-2}$$

And solving for p will lead to the following the design condition expressed by the following inequality.

$$p < \frac{\lambda_0}{2} \tag{3-3}$$

In simpler words, the mode $n = -1$, which is considered as a fast mode enforces some design principles on leaky wave antennas. This fast mode actually excites other slow modes and leads to wave propagation from the antenna while part of the EM wave leaks out of each slot as the wave travels along the structure. The frequency range for simulation is between $f = 2\ GHz$ to $f = 6\ GHz$. This antenna could be designed with a considerably thin substrate to increase the conformity of the structure.

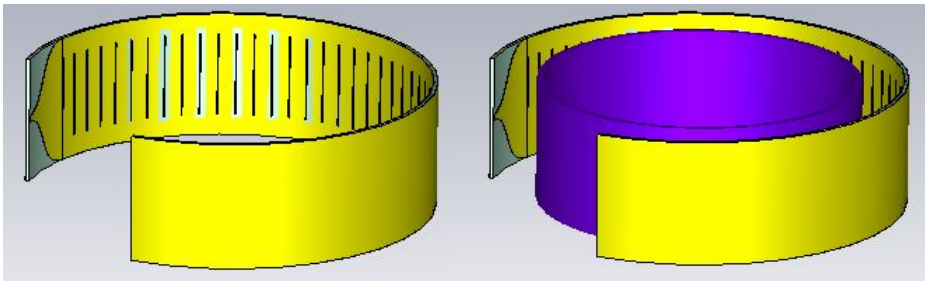

(a) **(b)**

Figure 3.5. The structure of ring-shaped leaky wave antenna (a) Ring-shaped leaky wave antenna without tissue (b) Ring-shaped leaky wave antenna with tissue.

Figure 3-6 illustrates the propagation pattern of this antenna at 2.45 GHz as well as the return loss graph.

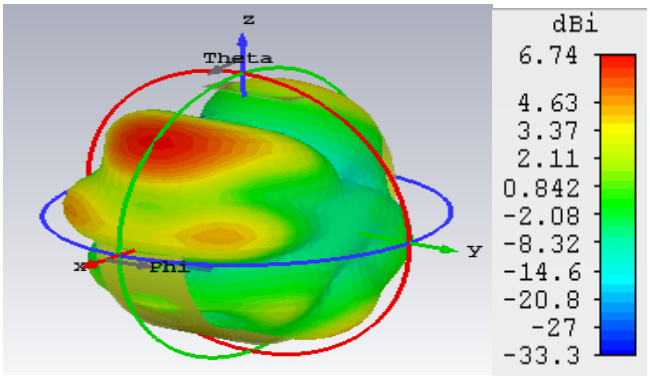

(a)

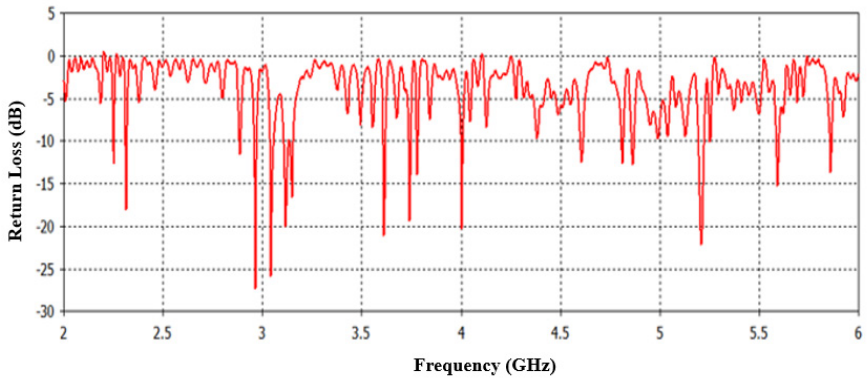

(b)

Figure 3.6. Propagation pattern of ring-shaped LWA at 2.45 GHz (b) Return loss graph.

3.3 Specific Absorption Ratio and Methodology

SAR gives a measure of the rate of the absorption of energy by a human body tissue. This measure can be expressed by electric field intensity or temperature variation as shown in equation 3-4.

$$SAR = \frac{\sigma |E_{inc}|^2}{2\rho} \tag{3-4}$$

In which, σ is the conductivity of tissue, E_{inc} is the electric field intensity of the incident wave and ρ is the density of tissue. In simpler words, SAR is defined as the average power loss density or $\sigma |E_{inc}|^2$ in density volume of a given tissue in human body or ρ. It is important to note that a given tissue is composed of 4 layers: bone, muscle, fat and skin. In the CST Studio Suite which is the software package used for acquiring SAR results, actually in simulation steps we set field monitors for calculation of power loss density as explained in the formula above and finally the software is able to give us the specific absorption ratio as thermal maps that are expressed in $Watt/Kg$ (Watt per Kilogram of a tissue).

There are different ways for SAR analysis in CST software such as average SAR and point SAR. In the average SAR, basically a cube of 1g or 10g is considered and power loss density is calculated for this whole 3D region. In point SAR the software allocates a SAR value to a given point without doing any averaging. The following table shows the maximum of mass averaged SAR values that are acceptable world-wide [12]. The results of this work are based on US and Canada standards which suggest to have average SAR values below 1.6 [W/kg].

Table 3.2. Specific absorption ratio guide.

Typical Standards	**SAR Limit (W/Kg)**
US & Canada	1.6 (W/Kg) averaged over 1g of tissue
EU, Japan, Brazil	2 (W/Kg) averaged over 10g of tissue

There are mature SAR methods that are developing rapidly but it is still challenging for any of these methods to make a precise prediction of heat distribution in human body tissues, because the thermal characteristics of a given tissue might differ from patient to patient and from this tissue to that tissue. Thus; that leaves some uncertainty in the prediction using these equations. One of the most famous bioheat equations is called the Pennes Bioheat equation that is expressed as follows [13].

$$\rho * c * \frac{\partial \mathrm{T}}{\partial \mathrm{t}} = \nabla.(\mathrm{k}\nabla \mathrm{T}) + \rho * Q + \rho * SAR - \rho_b * c_b * \rho * \omega * (T - T_b) \quad (3\text{-}5)$$

In which, c is the specific heat capacity, T is temperature, t is the time, ρ is volume density, Q is the metabolic heat rate, SAR is the specific absorption ratio, ρ_b is the blood mass density, c_b is the specific heat capacity of blood, ω is the blood perfusion rate and T_b is the blood temperature which could be considered as $37\,^{\circ}C$. We developed an image processing tool in MATLAB that is able to extract the geometry of the heated area (in 2D) and calculate the affected area in mm-squared using the SAR map. Using this MATLAB code, gives us a good insight into the heating mechanism and the type of heat distribution that each of the leaky wave antennas could apply to a given tissue.

3.4 Results and Discussion

In this research work, 1g average SAR and point SAR were simulated and the sample tissue used was a sheet of kidney tissue in form of a square block. In the point SAR the local SAR is calculated but without any mass or volume averaging while in the average SAR, after the calculation of the local SAR the value is divided by a fixed volume. In each case the tissue was placed in near field of the antenna, the antenna was excited using a Gaussian excitation and the Time domain solver of CST was used to get the EM results including propagation patterns, return loss, VSWR and especially the power loss densities at the given frequencies. By having the power loss densities at each frequency, we then used the Template Based Postprocessing to extract SAR maps, where we had the option to choose between 1g average SAR and point SAR. For each antenna type, the 4 frequency points $f = 2GHz, f = 2.45, f = 3GHz$ & $f = 3.6GHz$ are considered. The main frequency point would be 2.45 GHz to be compatible with the allocated frequency band suggested by FCC but the authors thought it is informative to have more frequency points at higher bands to be able to study thermal distribution on the tissue at other frequencies in addition to the medical band. The tissue area is a constant number of $A = 2.5504 * 10^4\ mm^2$ for the mushroom type and 2D periodically slotted leaky wave antennas.

In the following part, the SAR analysis results are illustrated. There are 8 figures for each antenna. Figures coded with (a) are showing average SAR results and figures coded with (b) are showing point SAR results. SAR values are summarized in the corresponding tables for each set of results. Here are the results for the mushroom-type leaky wave antenna. It is interesting to see how the geometry of the heat distribution changes when we switch from one frequency to the other. For example, by looking at figures 3-7 and 3-8, we can see how the shape of the heat distribution areas change by switching from 2 GHz to 2.45 GHz. At 2.45 GHz the pattern looks like a four-leaf clover which could be useful when several adjacent areas of a given tissue are to be targeted for treatment. So, the authors think that depending on what pattern is created by which antenna and at which frequency, the medical doctors could switch between 2 or more different types of antennas as different tools for hyperthermia therapy.

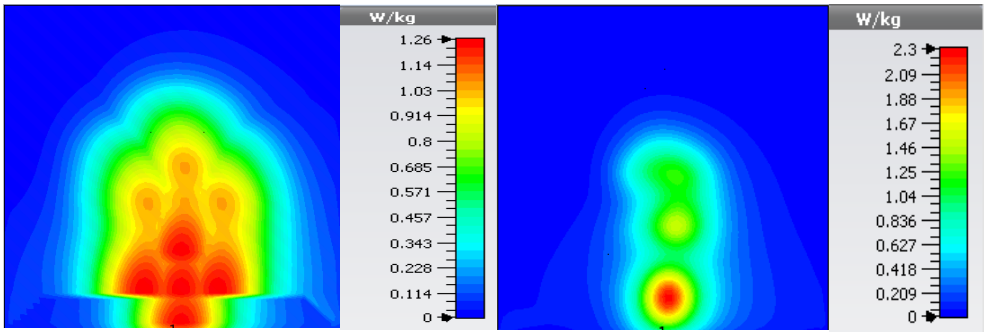

(a) **(b)**

Figure 3.7. SAR map [W/kg] of Mushroom-type LWA on kidney tissue at 2 GHz (a) 1g average SAR (b) point SAR.

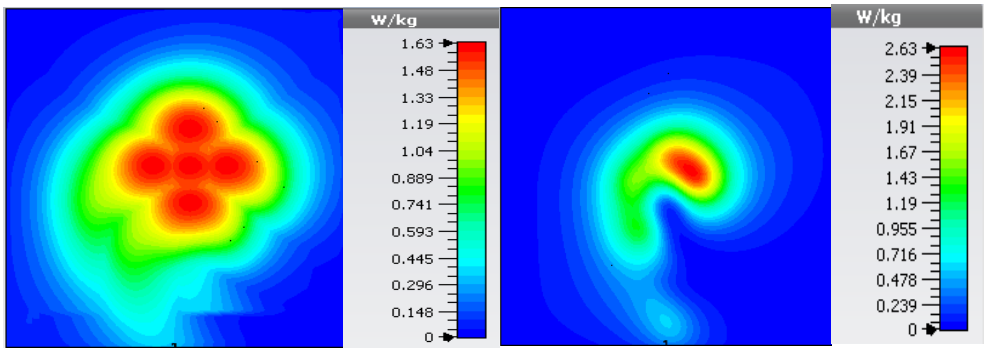

(a) **(b)**

Figure 3.8. SAR map [W/kg] of Mushroom LWA on kidney tissue at 2.45 GHz (a) 1g average SAR (b) point SAR.

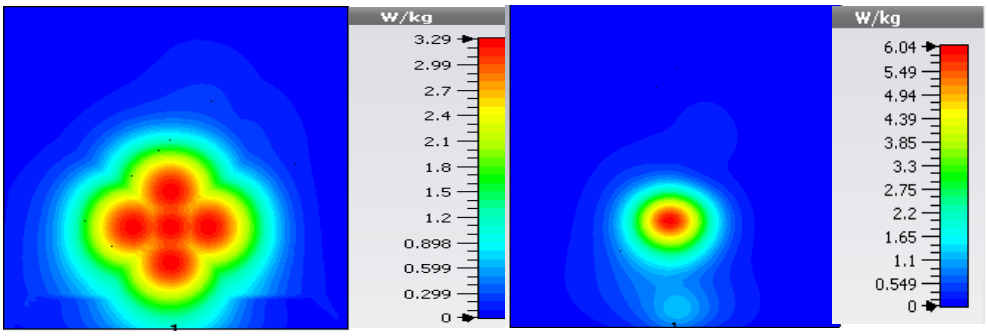

(a) **(b)**

Figure 3.9. SAR map [W/kg] of Mushroom LWA on kidney tissue at 3 GHz (a) 1g average SAR (b) point SAR.

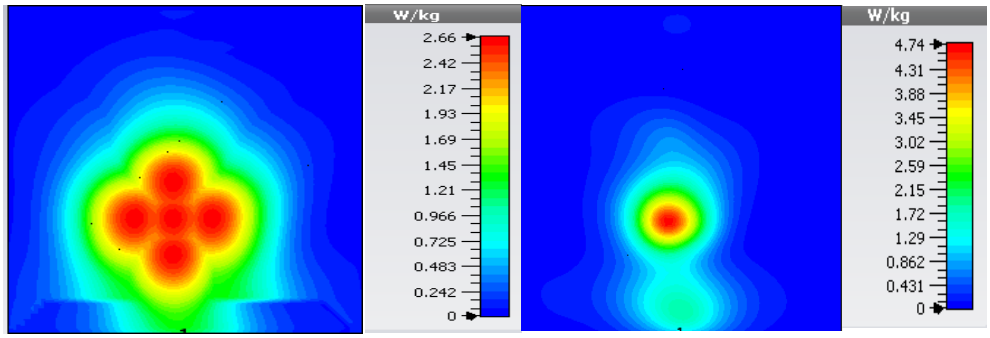

(a) **(b)**

Figure 3.10. SAR map [W/kg] of Mushroom LWA on kidney tissue at 3.6 GHz (a) 1g average SAR (b) point SAR.

Table 3.2. SAR values for Mushroom-type LWA.

Frequency (GHz)	**1g Average SAR [W/kg]**	**Point SAR [W/kg]**
2	1.26	2.3
2.45	1.63	2.63
3	3.29	6.04
3.6	2.66	4.74

In this section, we can see the SAR analysis results for 2D periodically slotted leaky wave antenna with double-permittivity substrate. Exactly at 2.45 GHz, we can see two heated areas that look like cross in figures 3-11 to 3-13. By switching from 2.45 GHz to 3GHz the affected area transforms itself from a more homogeneously heated region such as in figure 3-12 to a more focused format such as in figure 3-13, which could be applicable to a scenario whereby a more concentrated beam is required for treatment.

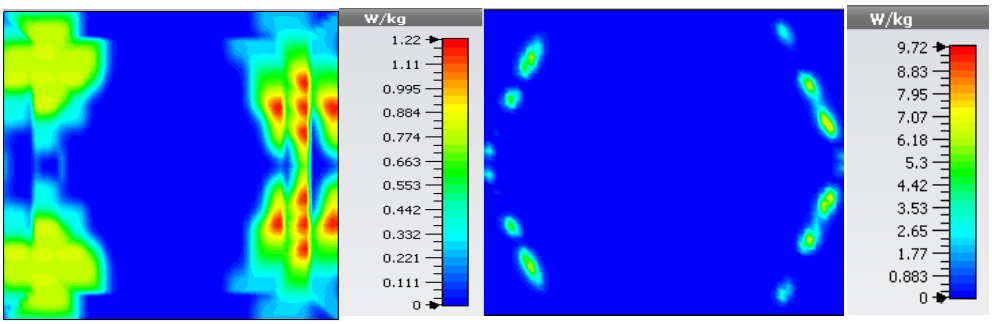

(a) **(b)**

Figure 3.11. SAR map [W/kg] of 2D periodically slotted LWA on kidney tissue at 2 GHz (a) 1g average SAR (b) point SAR.

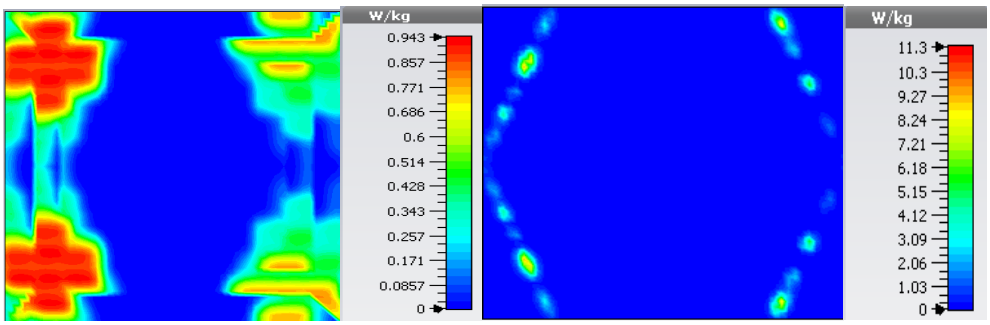

(a) **(b)**

Figure 3.12. SAR map [W/kg] of 2D periodically slotted LWA on kidney tissue at 2.45 GHz (a) 1g average SAR (b) point SAR.

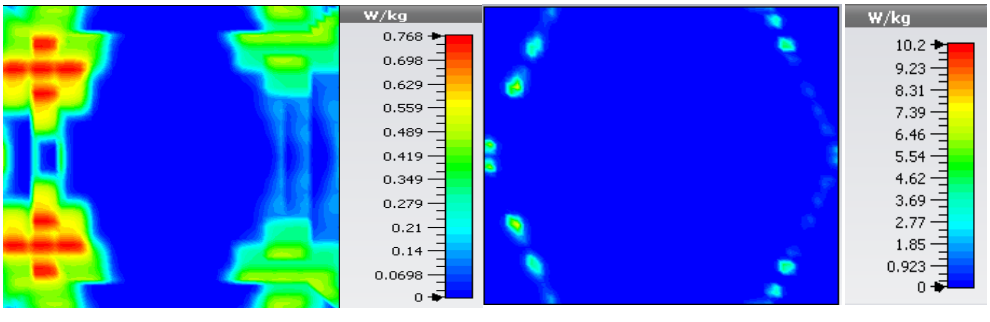

(a) **(b)**

Figure 3.13. SAR map [W/kg] of 2D periodically slotted LWA on kidney tissue at 3 GHz (a) 1g average SAR (b) point SAR.

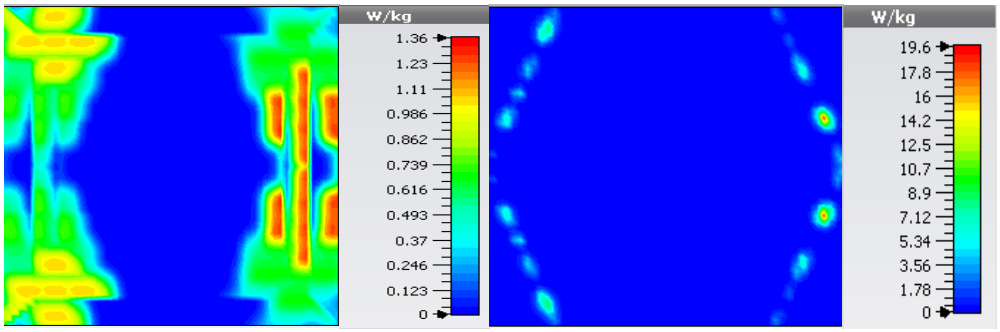

(a) **(b)**

Figure 3.14. SAR map [W/kg] of 2D periodically slotted LWA on kidney tissue at 3.6 GHz (a) 1g average SAR (b) point SAR.

Table 3.3. SAR values for of 2D periodically slotted LWA.

Frequency (GHz)	**1g Average SAR [W/kg]**	**Point SAR [W/kg]**
2	1.22	9.72
2.45	0.943	11.3
3	0.768	10.2
3.6	1.36	19.6

This section illustrates the SAR results for belt-shaped leaky wave antenna. In this case, the tissue geometry has been chosen to be a washer. In other words, a cylinder with the inner radius of 73mm and outer radius of 76 mm and height of 60mm. The reason for considering such geometry for the tissue under study is that, one could see the heat distribution in the inner and outer walls of this geometry better. Of course, it is also possible to consider the tissue as a filled cylinder. The surface area of this geometry is calculated to be $A = 1.4326 * 10^4\ mm^2$ for each side. As we can see on figures 3-15 to 3-17, the geometry of the heated area changes from extended region in figure 3-15 to focused heat pattern on figure 3-17.

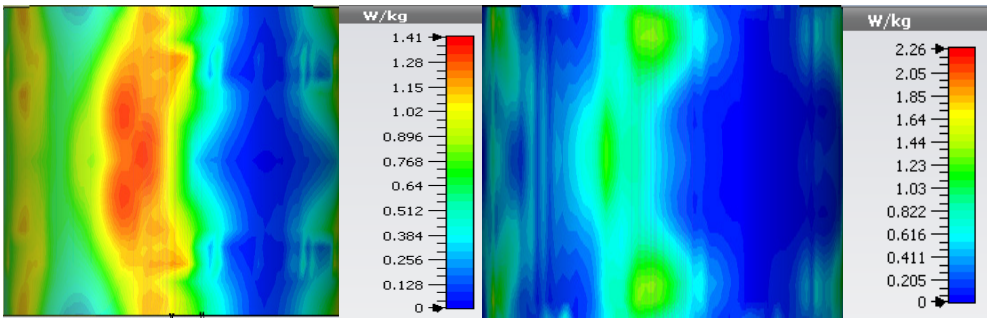

(a) **(b)**

Figure 3.15. SAR map [W/kg] of belt-shaped LWA on kidney tissue at 2 GHz (a) 1g average SAR (b) point SAR.

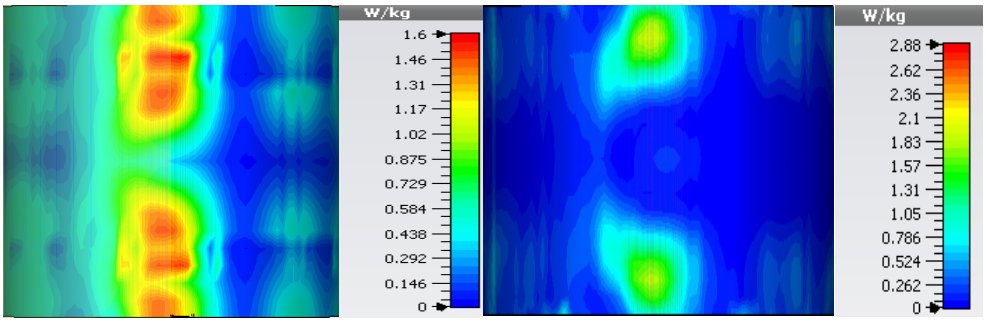

(a) **(b)**

Figure 3.16. SAR map [W/kg] of belt-shaped LWA on kidney tissue at 2.45 GHz (a) 1g average SAR (b) point SAR.

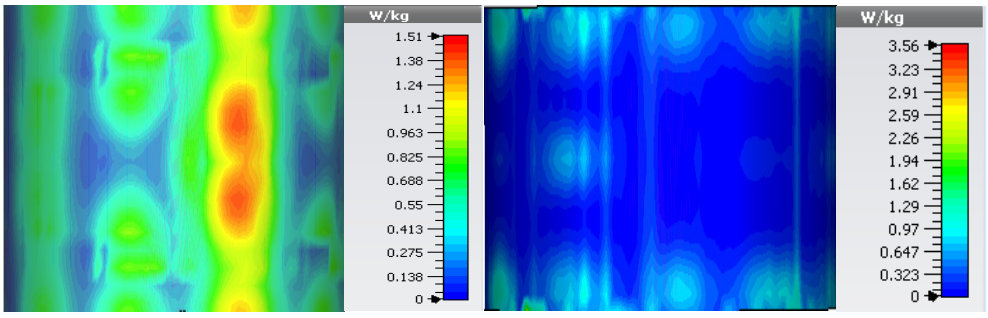

(a) **(b)**

Figure 3.17. SAR map [W/kg] of belt-shaped LWA on kidney tissue at 3 GHz (a) 1g average SAR (b) point SAR.

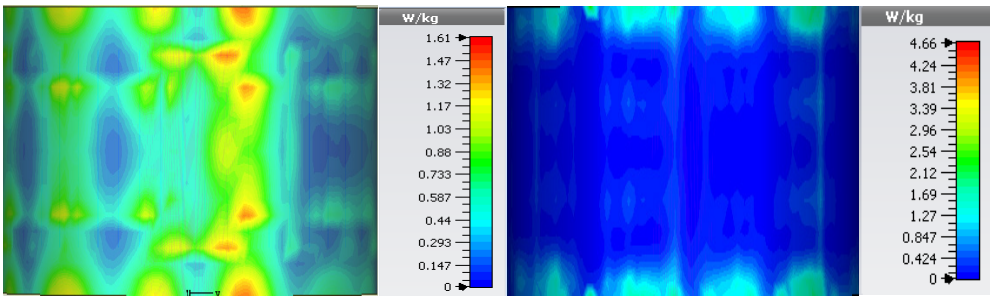

(a) **(b)**

Figure 3.18. SAR map [W/kg] of belt-shaped LWA on kidney tissue at 3.6 GHz (a) 1g average SAR (b) point SAR.

Table 3.4. SAR values for belt-shaped LWA.

Frequency (GHz)	**1g Average SAR [W/kg]**	**Point SAR [W/kg]**
2	1.41	2.26
2.45	1.6	2.88
3	1.51	3.56
3.6	1.61	4.66

In the following section, we are going to discuss the SAR results after applying image processing code to them. The MATLAB code is able to filter out the main heated area and calculate the affected area in mm^2. The logic of this program follows the RGB coding, in which one needs to set thresholds for red, blue and green values. Setting those thresholds could define what range of 'red' is acceptable for the current application. Numbers 0 to 255 are allocated to colors and each color can be defined as mixture of red, blue and green, thus we could attribute an array of 3 numbers to any color. For example, 'pure red' is (255,0,0), etc.

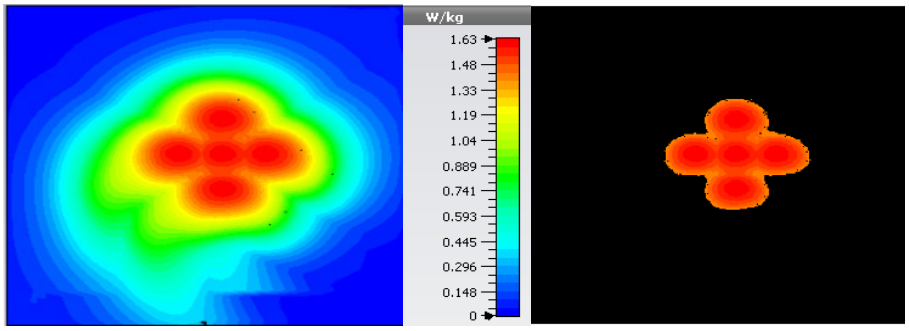

(a) **(b)**

Figure 3.19. SAR map [W/kg] of mushroom LWA on kidney tissue at 2.45 GHz (a) 1g average SAR map (b) filtered SAR map.

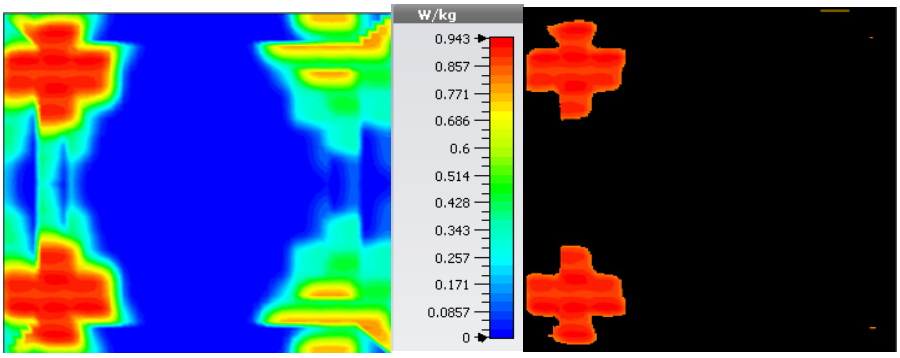

(a) **(b)**

Figure 3.20. SAR map [W/kg] of 2D periodically slotted LWA on kidney tissue at 2.45 GHz (a) 1g average SAR map (b) filtered SAR map.

Table 3.5. Heated tissue area calculation.

Antenna Type	**Heated area in mm^2**
Mushroom-type LWA	1.998484e+03
2D periodically slotted LWA	2.389691e+03
Ring-shaped LWA	3.191384e+02

3.5 Conclusion

Three novel leaky wave antennas were introduced in this paper for application in microwave hyperthermia. These antennas are 2D Mushroom-type leaky wave antenna, 2D periodically slotted leaky wave antenna and belt-shaped leaky wave antenna. Each of these microwave systems offer some distinguished frequency scanning and microwave ablation properties along with efficient performance which make them appealing for treatment of different tumors in different body parts. The proposed antennas in this paper work within the medical frequency band of 2.45 GHz. To verify the functionality and efficiency of each design, the thermal analysis using specific absorption ratio graphs was done using CST Studio software.

3.6 References

[1] Hegyi, Gabriella, Gyula P. Szigeti, and András Szász. "Hyperthermia versus oncothermia: cellular effects in complementary cancer therapy." Evidence-based complementary and alternative medicine: eCAM 2013 (2013).A. Z. Elsherbeni, FDTD Course Notes, Department of Electrical Engineering, The University of Mississippi, MS, Spring 2001.

[2] He, Xiaoping, Wen Geyi, and Shenyun Wang. "A hexagonal focused array for microwave hyperthermia: optimal design and experiment." IEEE Antennas and Wireless Propagation Letters 15 (2015): 56-59.

[3] P. F. Tumer, T. Schaefermeyer, M. Latta, R. Lauritzen, and D. T. Sells, ‘‘3-D heating pattern steering using the sigma eye phased array applicator controlled by a modified BSD-2000 Hyperthermic Oncology,’’ edited by C. Franconi et al. (Tor Vergata Post Graduate School of Medical Physics, Rome), 1996, pp. 571–573.

[4] Debnath, Oiendrila B., et al. "Design of invasive and non-invasive antennas for the combination of microwave-hyperthermia with radiation therapy." 2015 IEEE MTT-S 2015 International Microwave Workshop Series on RF and Wireless Technologies for Biomedical and Healthcare Applications (IMWS-BIO). IEEE, 2015.

[5] Sabariego, Ruth V., Luis Landesa, and Fernando Obelleiro. "Synthesis of an array antenna for hyperthermia applications." IEEE transactions on magnetics 36.4 (2000): 1696-1699.

[6] Paulides, Margarethus M., et al. "A patch antenna design for application in a phased-array head and neck hyperthermia applicator." IEEE Transactions on Biomedical Engineering 54.11 (2007): 2057-2063.

[7] M. M. Paulides, S. H. J. A. Vossen, A. P. M. Zwamborn and G. C. Van Rhoon, "Theoretical investigation into the feasibility to deposit RF energy centrally in the head and neck region", Int. J. Rad. Onc. Biol. Phys., vol. 63, pp. 634-642, 2005.CST Microwave Studio, ver. 2008, Computer Simulation Technology, Framingham, MA, 2008.

[8] M. M. Paulides, J. F. Bakker, A. P. M. Zwamborn and G. C. Van Rhoon, "A head and neck hyperthermia applicator: Theoretical antenna array design", Int. J. Hyperthermia, vol. 23, no. 1, pp. 59-67, 2007.

[9] Luyen, Hung, Susan C. Hagness, and Nader Behdad. "A balun-free helical antenna for minimally invasive microwave ablation." IEEE Transactions on Antennas and Propagation 63.3 (2015): 959-965.

[10] M. Sarabi and W. Perger, "A Novel Leaky Wave Antenna for Hyperthermia," 2019 IEEE Texas Symposium on Wireless and Microwave Circuits and Systems (WMCS), Waco, TX, USA, 2019, pp. 1-4, doi: 10.1109/WMCaS.2019.8732516.

[11] Hamed, Tooba, and Moazam Maqsood. "SAR Calculation & Temperature Response of Human Body Exposure to Electromagnetic Radiations at 28, 40 and 60 GHz mmWave Frequencies." Progress In Electromagnetics Research 73 (2018): 47-59.

[12] Wittig, T., “SAR overview,” www.cst.com, accessed Nov. 25, 2016.

[13] https://www.sciencedirect.com/topics/medicine-and-dentistry/specific-absorption-rate.

4 A Novel Comb-line Leaky Wave Antenna for FMCW Automotive Radar

4.1 Introduction

Road safety has always been a challenging issue and unfortunately, there are a considerable number of deaths or injuries that happen to both drivers and pedestrians each year. The National Highway Traffic Safety Administration (NHTSA) is an agency in the United States which provides precise reports and statistics on road casualties and fatalities that happen on the roads throughout US. Figure 4-1 shows the statistics of fatalities provided by NHTSA from 1975 to 2019. As we see, in 2019 alone there were 36,096 fatalities on the US roads [1].

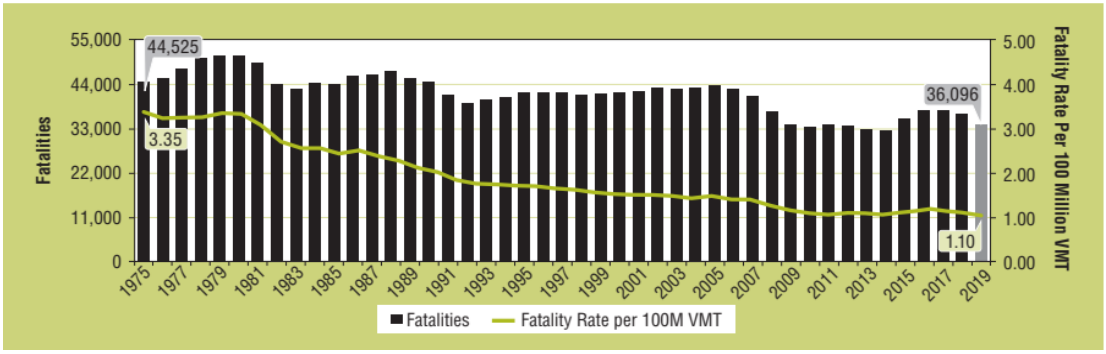

Figure 4.1. Fatalities and Fatality Rate per 100 Million VMT, 1975-2019 [1].

Different solutions have been so far proposed to increase the road safety. But amongst the proposed methods, frequency modulated continuous wave (FMCW) radars are one of the most promising solutions compared to other types of automotive radar systems. These radars are low-cost, simple in architecture and also have robustness in foggy or rainy weather which make them more appealing compared to LIDAR or camera. In general, there are two types of radars: pulse radars and continuous wave (CW) radars. In pulse radars, we transmit a very short pulse accompanied by high average power. Each pulse period has two portions: in the first portion the radar simply sends signals and in the second portion no pulse is sent and the radar waits or 'listens' for receiving the echoes of targets. Since in pulse radars the time signal is rather short, we would then have a high bandwidth in the frequency domain (by considering the Fourier transform) and thus based on equation 4-1,

we could have a decent range resolution, ΔR, where c is the speed of light and bw is the bandwidth:

$$\Delta R = \frac{c}{2 * bw} \tag{4-1}$$

Unlike pulse radars, continuous wave radars, as the name implies, continuously send radar signal towards targets. In CW radars the peak-to-average power is quite low (a few watts) and this factor makes such radars more economical for automotive applications compared to the pulse-waveform radars [2]. There are many interesting applications or aspects of FMCW radars to be yet improved. For example, in [3], the authors mention FSK radars and their disadvantage of having low distance resolution despite having good speed resolution, which makes it tricky to distinguish between 2 targets with more or less the same speeds. Therefore, they use linear frequency modulation (LFM) format to deal with complicated scenarios and introduce an FMCW radar system with functionality as adaptive cruise control (ACC) at 77GHz. In [4], the emphasis is on the design of a baseband signal processing system for FMCW radar. The authors, introduce a 3-ramp chirp in which the third ramp actually acts as a check ramp. This has an advantage of increasing accuracy and shortening the measurement time without making RF front-end more complex. However, in the literature such as [3] and [4] the focus is mostly on the signal processing and detection algorithm parts, while in [5] and [6] the center of attention is on the application of antenna system of the proposed FMCW radar systems. In [5] the authors have introduced a 60 GHz leaky wave antenna that is used to do simultaneous estimation of the direction of arrival (DOA) and ranging of multiple objects that provides 60° beam steering by sweeping from 50 GHz to 60 GHz. While in our design we have reached a higher beam steering angle range while using smaller frequency sweep range discussed in section III. There is already a proposed microstrip leaky wave antenna to track the humans [6].

One of the most challenging issues in multi-target radar systems is the existence of ghost targets. Any radar detection other than the main targets is considered as ghost target. It could have different causes and so the solutions are as diverse as the types of ghost targets themselves. For example, in [7] the ghost targets are caused by inter-radar interference and

to suppress such ghost targets, authors use a carrier sensing method and interference replica to suppress the ghosts. In our proposed system there is an easy solution which will be discussed in section IV.

The antenna that is used in any radar system is one of the main factors that determines the overall cost of the system. In this work we have studied the application of a comb-line leaky wave antenna for radar systems to explore the interesting characteristics of these antennas. Leaky wave antennas are broadband, simple in structure and with capability of beam scanning which make them rather appealing for radar system applications. Equation (2) explains the mechanism of beam scanning in 1D leaky wave antennas, where θ_m is the direction of the main beam, $\beta(f)$ is the propagation constant which is a function of frequency and k_0 is the free-space wave number:

$$\sin(\theta_m) = \frac{\beta(f)}{k_0} \tag{4-2}$$

Thus, once the excitation frequency of a leaky wave antenna changes, the propagation constant changes which in turn shifts the angle of the main beam and actually functions as a beamforming technique. In fact, leaky wave antennas are modified waveguiding structures. Modifications such as periodic slots or stubs that allow the electromagnetic wave to leak through them as it travels along the structure, give leaky wave antennas such interesting properties [8].

The mechanism of wave leakage through each periodic slot was first explained by Hyneman in [9]. In Hyneman's work, the Floquet periodicity theorem [10] was applied to periodic leaky wave antennas whereby the field of each slot could be expanded as a multiplication of a periodic function by general exponential wave function of the form e^{-jkz}, in which z is the direction of the wave travel. The structure of this paper is as follows: section II discusses the generic mathematics behind FMCW radars, section III discusses our proposed multi-target radar system as well as the main building blocks of this design, section IV includes signal processing and radar detection, section V discusses the evaluation of our proposed leaky wave antenna as the FMCW radar system's antenna

versus antenna arrays that are typically used in radar systems and finally section VI, concludes this paper.

4.2 Frequency Modulated Continuous Waveforms

A typical FMCW radar system is shown in figure 4-2 which includes the following block diagrams of transmitter, receiver, mixer and analogue to digital converter (A/D).

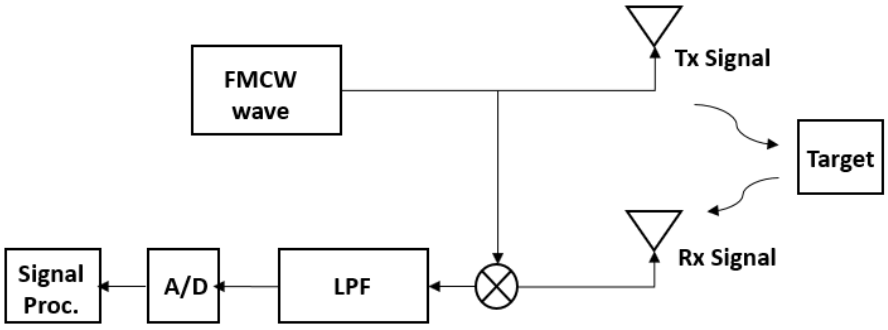

Figure 4.2. Schematic of a generic FMCW Radar system.

In simple words, an FMCW signal is generated at the transmitter side and sent via transmitter antenna towards the receiver. At the receiver's side, after receiving the echo signal reflected from a target, a mixer combines the chirp signal (reference signal) and the reflected signal. A low pass filter removes the higher frequency harmonics and keeps the intermediate frequency (IF) signal which then goes to the analogue-to-digital converter and finally to the signal processing block for detection and range-Doppler mapping.

4.2.1 FMCW Signal Model

The transmitted signal can be considered as:

$$s_{tx}(\mathrm{t}) = A_{tx} \cos(2\pi f_c t + 2\pi \int_0^t f_{tx}(\tau) d\tau) \qquad (4\text{-}3)$$

In which, $f_{tx}(\tau) = \frac{B}{T}.\tau$ is the linear chirp function of the transmit frequency while chirp could be exponential, quadratic, etc. but in this work the linear chirp is used, f_c is the

working frequency of radar, B is the bandwidth, A_{tx} is the signal amplitude and T is the pulse duration. On the other hand, the receiving frequency is:

$$f_{rx}(t) = \frac{B}{T}\,(\mathrm{t} - t_d) + f_D \tag{4-4}$$

Where t_d being the time delay and a target moving with the velocity v gives the Doppler shift f_D is expressed as equation 4-5.

$$f_D = -2\,\frac{f_c v}{c} \tag{4-5}$$

The parameter c is the speed of the light. We could consider the received signal $s_{rx}(t)$ as equation 4-6.

$$\begin{aligned} s_{rx}(t) &= A_{rx}\cos(2\pi f_c(t - t_d) + 2\pi \textstyle\int_0^t f_{rx}(\tau)d\tau) \\ &= A_{rx}\cos\{2\pi\,(f_c(t - t_d) + \tfrac{B}{T}\left(\tfrac{1}{2}t^2 - t_d.t\right) + f_D.t)\} \end{aligned} \tag{4-6}$$

Where A_{rx} is the amplitude of the received signal that is influenced by the radar cross section (RCS), distance of the target, gains of transmitting and receiving antennas and also the power used for the transmission. As figure 4-2 illustrates, once the FMCW signal is generated at the transmitter's side, a branch of this signal is injected into the mixer that is at the receiver's side. In this mixer the reference signal and the received signal (echo from the target) are mixed together or in other words they are multiplied together which generates higher frequency components in addition to lower frequency ones. In order to suppress the higher frequency components and get the IF signal (intermediate frequency signal), a low pass filter is used right after the mixer. The IF signal is represented by $s_{IF}(t)$. If a triangular waveform which is composed of 2 ramps (a positive and negative ramp) is used, then 2 beat frequencies (f_{bu} and f_{bd}) will emerge after the LPF which are expressed in equations (6) and (7):

$$f_{bu} = \frac{2R_0}{c}.\frac{B}{T} + 2\,\frac{f_c v}{c} \tag{4-7}$$

$$f_{bu} = \frac{-2R_0}{c} \cdot \frac{B}{T} + 2\,\frac{f_c v}{c} \qquad (4\text{-}8)$$

The reflected signal that is coming back from a given target looks similar to the transmitted signal but in fact it is the shifted version of the reference signal both in time and frequency. Figure 4-3 illustrates the sent and the received spectrograms (Tx and Rx chirps correspondingly).

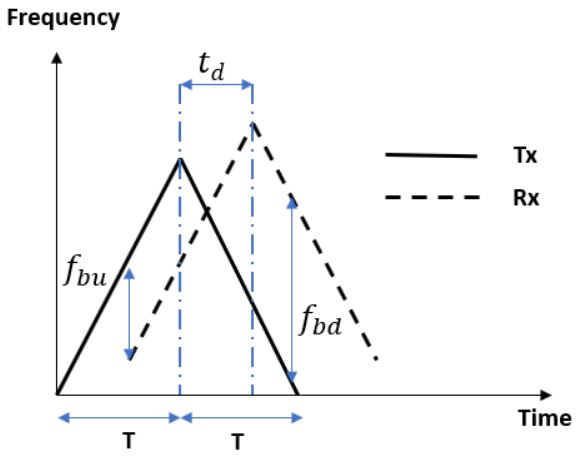

Figure 4.3. Spectrogram of the transmitted and received signals.

A chirp could also be in form of a sawtooth waveform as shown in figure 4-4.

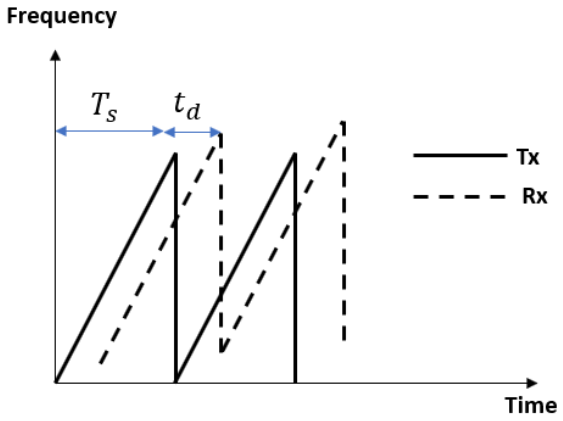

Figure 4.4. Spectrogram of the transmitted and received signals.

Based on this figure, we can write the following equations of the upbeat and downbeat frequencies.

$$f_b^+ = \frac{4\Delta f R}{cT_s} - f_D \tag{4-9}$$

$$f_b^- = \frac{-4\Delta f R}{cT_s} - f_D \tag{4-10}$$

Solving equations 4-9 and 4-10 for R and f_D, give the following equations:

$$R = \frac{cT_s}{8\Delta f}\frac{(f_b^+ - f_b^-)}{2} \tag{4-11}$$

$$f_D = -\frac{(f_b^+ + f_b^-)}{2} \tag{4-12}$$

4.3 The Proposed Radar Architecture

The proposed FMCW automotive radar system is shown in figure 4-5. The design parameters of the RF components of this system, such as system bandwidth, antenna gain, noise figure, etc. are summarized in table 4-1. The system design has been implemented using MATLAB Simulink.

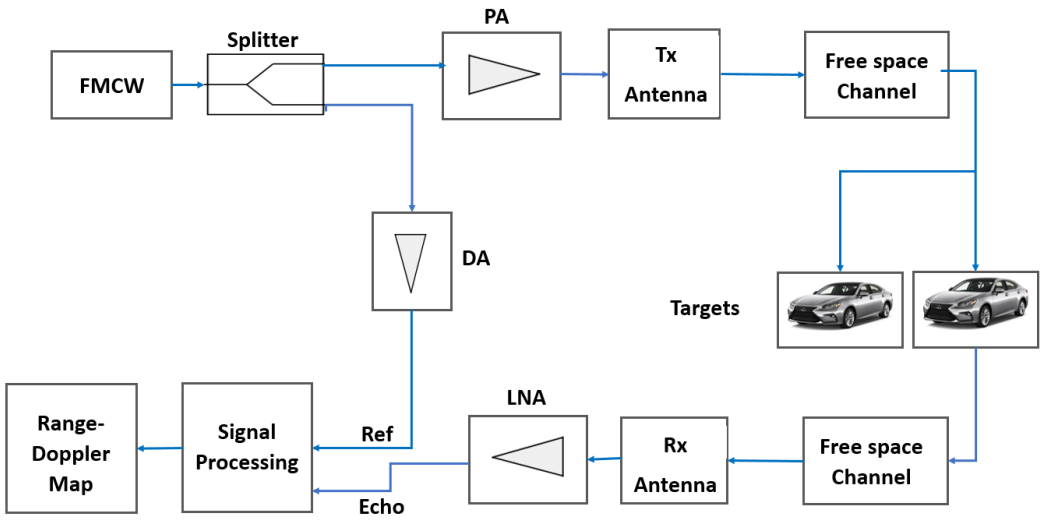

Figure 4.5. The architecture of the multi-target FMCW automotive radar

Table 4.1. RF Design parameters of the propose radar system.

Parameter	**Explanation**	**Value**
Fc	Carrier Frequency	77 GHz
Fs	Sampling frequency	150 MHz
BW	Bandwidth	150 MHz
Tx Gain	Transmitter's gain	36
Rx Gain	Receiver's gain	42
NF	Noise figure	4.5
NFFT	FFT length	2048
NDoppler	Doppler length	256
T	Period of chirp signal	7.33e-06

4.3.1 FMCW Signal Block

This block generates FMCW signal of 77 GHz frequency which is a typical frequency for automotive applications. We could use any type of chirp including linear, quadratic, etc. The linear chirp itself could be up, down or triangular. We have used both triangular and up-chirp in our proposed radar system.

4.3.2 Splitter

A splitter is a three-port and non-directional component that has the task of directing the input signal to two different outputs. A common type of splitter is the Wilkinson splitter.

4.3.3 Power Amplifier

This component is used to boost a weak signal into a strong signal as long as they are used in the linear region and the input signal doesn't cause the power amplifier to go to the saturation region.

4.3.4 Transmitter/Receiver Antenna

In this research, we propose the application of a leaky wave antenna as a substitute for an antenna array which is shown in figure 4-6 with the main dimensions. As we know, the automotive industry uses antenna array as a transmitting and receiving system. Leaky wave antennas have interesting properties that make them quite attractive for radar systems. By using the frequency scanning property of the leaky wave antennas, we could control the antenna beam in different directions as discussed in the introduction section.

The antenna proposed for this radar system is a comb-line leaky wave antenna with the substrate Arlon AD 350 with permittivity $\varepsilon_r = 3.5$. This Comb-line leaky wave antenna provides a simple beamforming structure and right/left-handed beam-scanning. The antenna structure is composed of 13 stubs to introduce periodicity and generate Floquet modes [4] and it is excited through 2 ports situated at both sides of the antenna. The technical design parameters are summarized in table (2). The antenna structure is composed of 31 stubs to introduce periodicity and generate Floquet modes [4] and it is excited through two ports situated at both sides of the antenna. The technical design parameters are summarized in table 4-2.

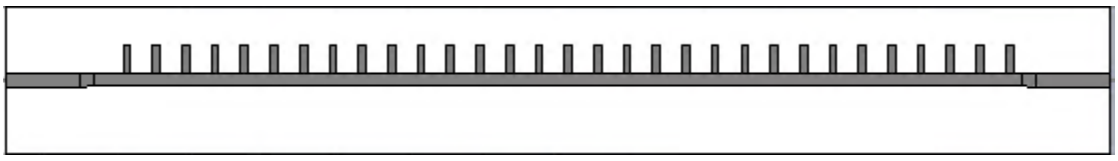

Figure 4.6. The Comb-line leaky wave antenna as FMCW radar antenna

Table 4.2. Design parameters of the comb-line LWA.

Parameter	**Symbol**	**Value**
Wavelength	λ	3.89
Microstrip width	W_m	1
Antenna length	L	75
Ground plane thickness	H_g	0.1
Stub width	W_{stub}	0.5
Stub length	L_{stub}	2
Period	p	2
Substrate thickness	H_s	0.38

The following table shows the frequency scanning property of the leaky wave antenna. The range of frequency sweep is between 75 GHz and 79 GHz and for each frequency point, the propagation pattern at plane $\varphi = 0^{\circ}$ has been calculated by CST Studio software package. By looking at the propagation patterns we can see that the comb-line leaky wave antenna has both left and right-handed propagations and there are beams with decent gains at these frequencies.

Table 4.3. Propagation patterns of the proposed comb-line leaky wave antenna at frequencies 75GHz, 77 GHz, 77.5 GHz and 79GHz.

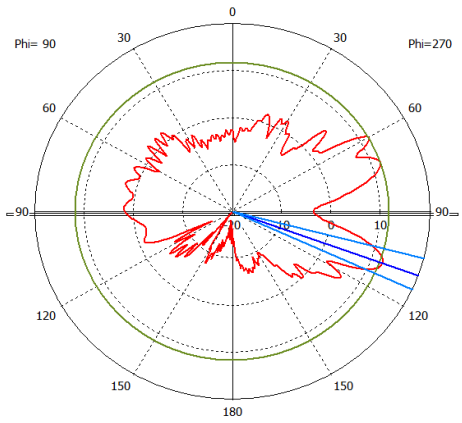	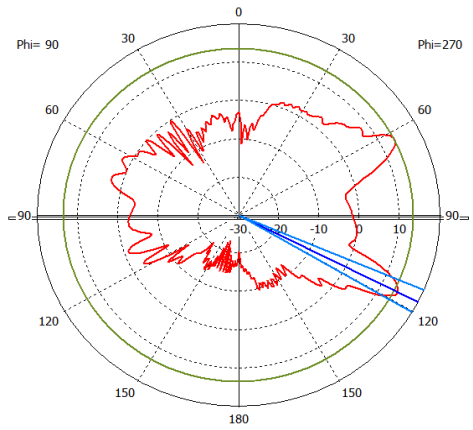
75 GHz	77 GHz
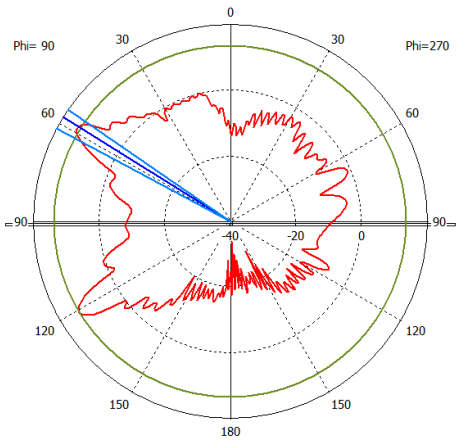	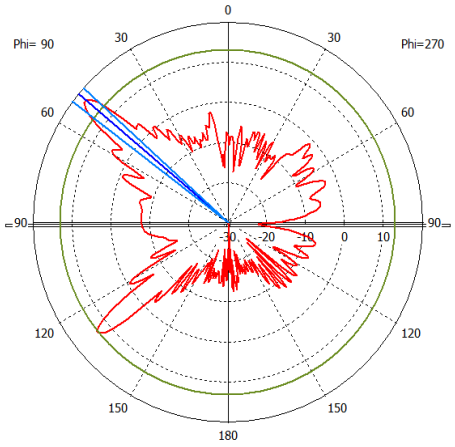
77.5 GHz	79 GHz

4.3.5 Propagation Channel

The propagation channel is considered to be a free space channel that is modeled by applying time delay as well as attenuation of the transmitted FMCW signal because of the path loss expressed in equation 4-13 where R is the propagation distance and λ the signal wavelength.

$$L_{pl} = \frac{(4\pi R)^2}{\lambda^2} \tag{4-13}$$

4.3.6 Target RCS

Every target could be attributed a radar cross section (δ) value. This parameter actually specifies how much the backscatter power per steradian is echoed from the target. In our radar design we considered 4 targets that could be matched with automotive application. The targets are a truck, a car, a motorcycle and a bike. There is an item in the target block which gives an option to consider fluctuation for a given target which leads to fluctuation loss and decrease of SNR. That is pointed out as Swerling models I, II, III, IV and V first introduced by the mathematician Peter Swerling. However, the fluctuating target could be of high importance for military applications and not necessarily for automotive applications.

Table 4.4. Radar cross sections of targets at f = 77 GHz.

Target	**RCS**
truck	1000
car	50
motorcycle	25
bike	15

4.3.7 Preamplifier

Preamp is a device for amplification and noise suppression of the echo signal. In the corresponding Simulink block, the attributed noise figure of this block is $NF = 4.5$ for the ambient temperature of $T = 290^{\circ}K$ and the gain is 42.

4.3.8 Signal Processing

The signal processing block is composed of 4 subblocks of mixer, pulse buffer, range-Doppler response and range-speed estimation. The mixer multiplies the reference signal with the echo signal which then generates IF signal. The pulse buffer block converts scalar samples to frame structure. The range-Doppler block receives the input IF signal and calculates range Doppler map using the FFT transform. The number of FFT points is 2048 in our platform. For range processing FFT windowing as well as Doppler processing FFT windowing we can use any of the 5 types of windows such as Hamming, Chebyshev, Hann, Kaiser and Taylor. Figure 4-7 summarizes the signal processing block and its subblocks.

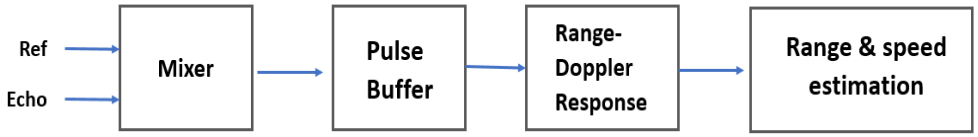

Figure 4.7. Subblocks of the signal processing block

4.4 Radar Detection

The proposed radar system was tested using 2 different FMCW chirps of sawtooth and triangular. The corresponding equations of both cases were discussed in section II (equations 6 - 11). In each case the evaluation of the radar system was done using range-Doppler map. In our simulations we assume that the radar system is installed on a reference vehicle that is moving with the speed of 27.77 m/s and the initial range of 0 m. The range–Doppler map actually gives us the relative velocity of a vehicle in relation to the radar as well as the relative range as equations 4-14 and 4-15 express.

$$\Delta v = v_{radar} - v_{vehicle} \tag{4-14}$$

$$\Delta R = R_{radar} - R_{Vehicle} \quad (4\text{-}15)$$

Table 4-5 summarizes the velocities and ranges of the considered targets (car, truck, motor and bike) as well as the expected relative velocity and relative range for each target.

Table 4.5. Targets' velocities and range values.

Target	**Target Velocity (m/s)**	**Target Range (m)**	Δv **(m/s)**	ΔR **(m)**
truck	36.11	65	-8.34	-65
car	16.66	65	+11.11	-50
motorcycle	35	45	-7.23	-45
bike	13	20	+14.77	-20

At the first stage, the triangular FMCW chirp was used in the radar system and the ghost target issue was challenging in this case. Since by increasing the number of the actual targets, the number ghost targets also increase. On the following pages, we have included the ghost target responses for each radar system. The horizontal axis is speed axis that is extended from -500 Km/h to +500Km/h. The vertical axis is range axis that extends from -500 m to +500 m and the color bar on the right-hand side of each graph is the power scale in dB scale. Based on our simulations, in the two-target scenario we observed 6 ghost targets as we can see on figure 4-8. In the three-target scenario the number of the ghost targets is 9 shown in figure 4-9 and correspondingly for the four-target scenario the number of the ghost targets is 12 shown in figure 4-10. It seems that for the proposed radar system when we use triangular chirp there is a linear equation that could be used to predict the number of ghost targets by plugging in the number of targets (N) as formulated in equation 4-16.

$$N_{ghost} = 3 * N \quad (4\text{-}16)$$

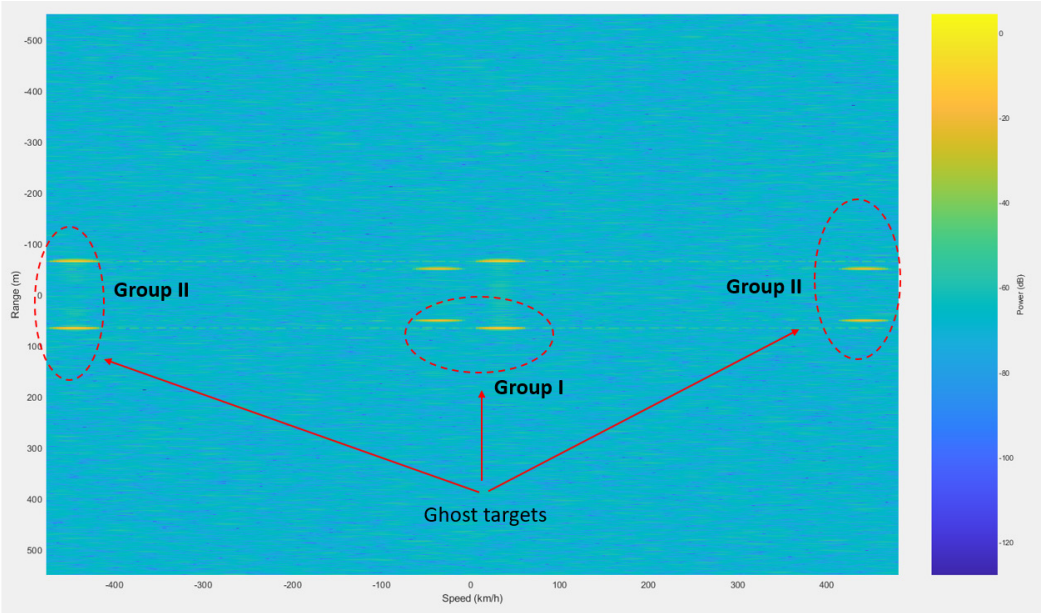

Figure 4.8. Range-Doppler map for 2-target scenario using triangular sweep

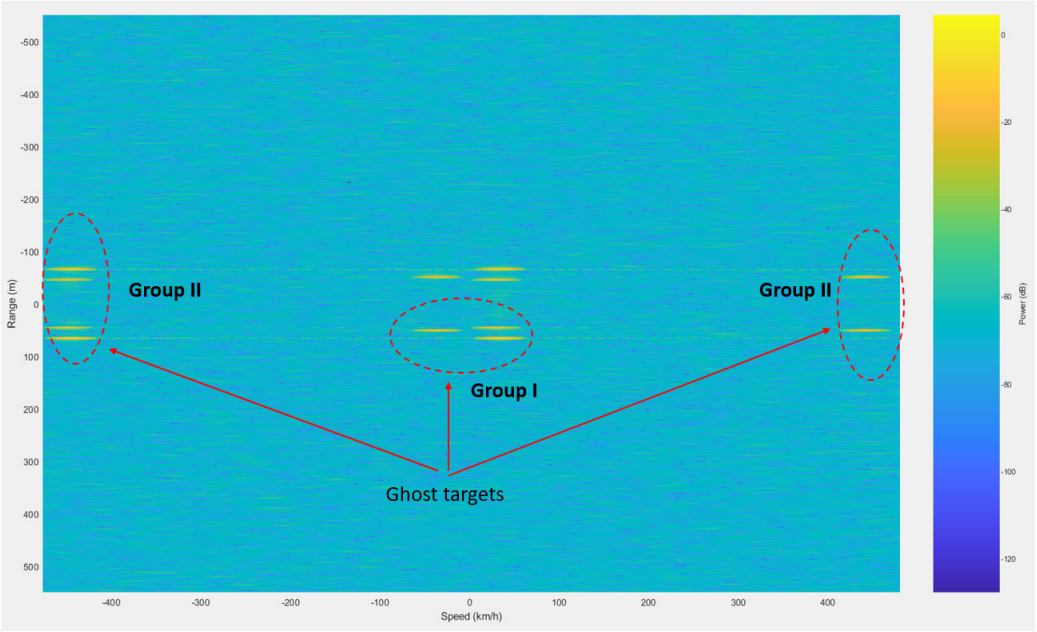

Figure 4.9. Range-Doppler map for 3-target scenario using triangular sweep

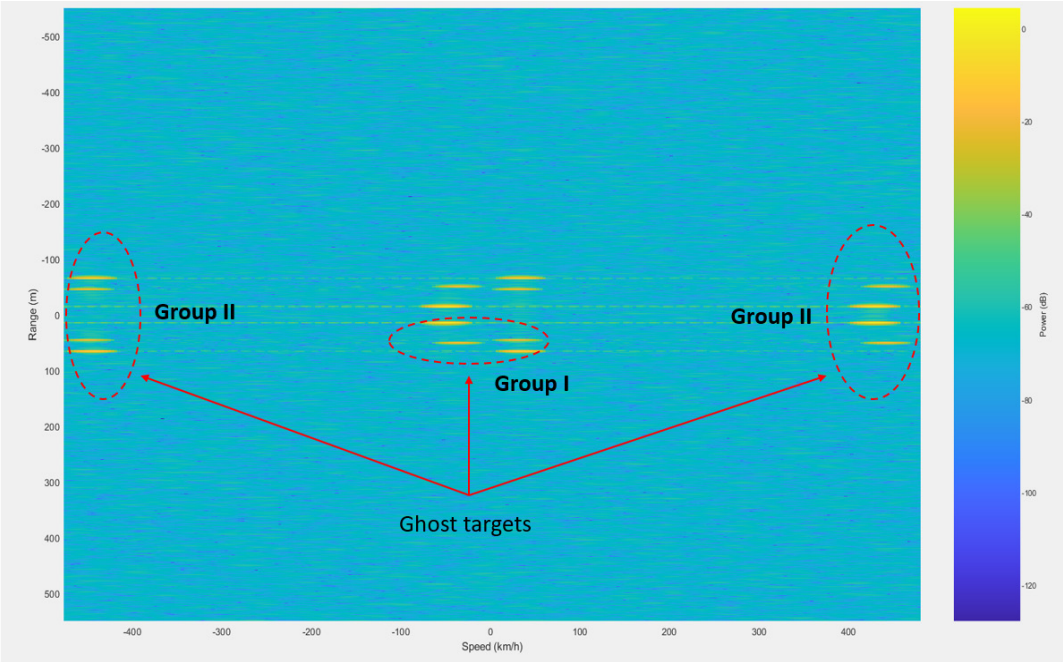

Figure 4.10. Range-Doppler map for 4-target scenario using triangular sweep

There are different methods for suppression of ghost targets (some literature review probably in the introduction section) but not every method works for every radar system. The authors think that in the triangular chirp the down-ramp causes some additional echoes and creates a scenario of "mirror ghosts". If we closely observe figures 4-8 to 4-10, we notice that there are two groups of ghost targets, the ghost targets that appear right below the actual targets marked as group 1 and the ghost targets that appear on the left- and right-hand side of the range-Doppler map marked as group II.

The ghost targets of group I are exactly the mirror of actual targets with reference to the range axis (axis of symmetry) and thus the velocities of group I's ghost targets are the same but the ranges are the opposite of the actual ones. It is even more interesting to see the ghost targets of group II. We can observe that some actual targets' echoes project themselves onto the left- and right-hand side of the range-Doppler map. By looking at the ghost targets of group II, we can see that they emerge on the two far ends of the map and mark very high velocities such as 400 km/h which can't be attributed to ordinary vehicles,

that we see on the roads. Thus, they can be easily neglected. But the ghost targets of group I could cause confusion in automotive scenarios since they are exactly within the same range of values or velocities as actual targets are. For our proposed system there is an easy fix and that is switching to the use of sawtooth chirp instead of the triangular chirp. Figure 4-11 illustrates that by switching to the sawtooth chirp the issue of the ghost targets is resolved.

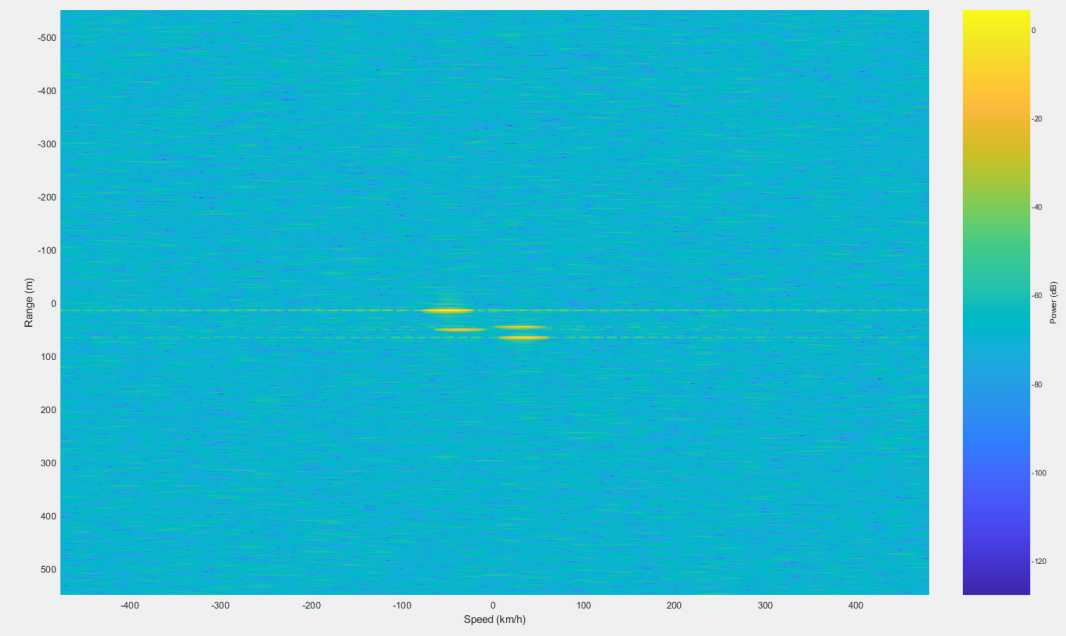

Figure 4.11. Range-Doppler map using sawtooth sweep

As a figure of merit for the range-Doppler graphs in our radar system, we can compare the power of the echo signal with the power of the background noise using the right-hand side color bars in figures 4-8 to 4-11. We can observe that basically our target returns have power of about -20dB or higher which is an easily detectable value against the background noise which is about -80dB.

4.5 Performance of the proposed LWA versus two antenna arrays

In this paper, several antenna arrays were designed and their performances were evaluated compared to our proposed leaky wave antenna. The small-signal S-parameters of each

design was extracted as Touchstone file since as we know, we can get the S-parameters of any microwave device with n ports, as snp where n shows the number of ports. CST Studio Microwave has the capability to extract the S-parameters in Touchstone format. For example, for our case, since we have only 2 feeding ports, the s2p file was extracted and directly plugged into the antenna blocks (transmitter and receiver) of the FMCW radar's architecture in Simulink.

4.5.1 Inset-fed Microstrip Patch Array

This structure is composed of 6 antennas as illustrated on fig. 4-12.

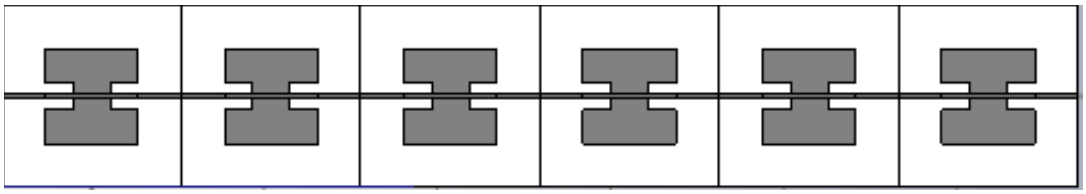

Figure 4.12. Range Inset-fed microstrip patch array

The main design parameters of a single cell of the array are summarized in table 4. The substrate used was Arlon AD 350 with permittivity value of $\varepsilon_r = 3.5$.

Table 4.6. Design parameters of the cell of the inset feed patch array.

Parameter	**Dimension (mm)**
Length of substrate	2.07
Width of substrate	2.07
Length of patch	1.08
Width of patch	1.10
Indentation Length	0.32
Indentation width	0.12

As we can see on Fig. 12, there is a decent resonance around the frequency of 77 GHz.

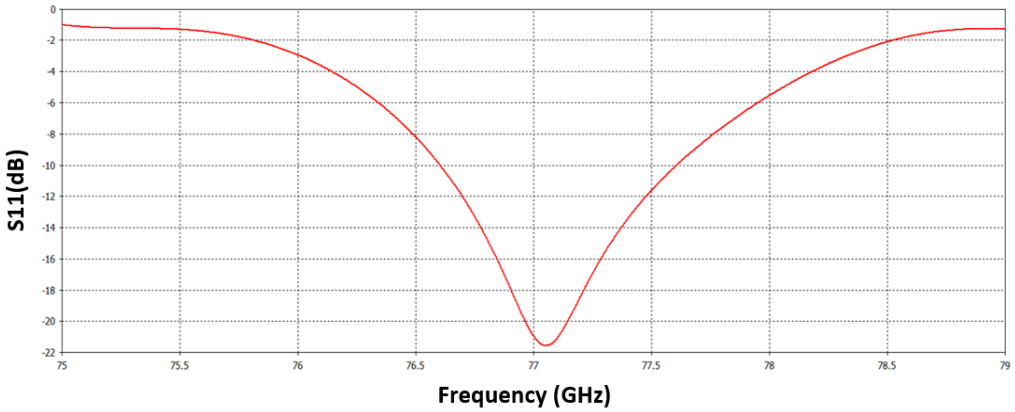

Figure 4.13. Return loss for port 1 of the inset feed patch array

Figure 4-14 shows the range-Doppler map of the radar system when we use inset-fed patch array. We have specified the 4 detected targets with red circles to be more obvious for the reader because in this case we believe by doing some antenna tuning and optimization in the designed array, we could possible improve the gain. In this case, the radar returns have power of -30dB which are still distinguishable against the background noise with -80dB power.

4.5.2 Circular Patch Array with Buttler Beamforming Network

Buttler beamforming networks are very common structures for beam scanning. These networks are comprised of branch-line couplers, cross-overs and phase shifters. In Figure 4-15, we can see different blocks of the Buttler matrix. Block A is a branch-line coupler which is a 90° or 45° hybrid coupler and we have four of the same couplers on the structure. Block B shows a microwave crossover. Block C shows a 45° phase shifter and we have two phase shifters on the matrix. Block D shows the circular patch antenna array which is considered for operation at 77GHz. The ports 1 to 4, on the left side of the Buttler matrix are actually the feed ports. At a given time, only one port is excited and three other ports are terminated using $50\ \Omega$ terminator.

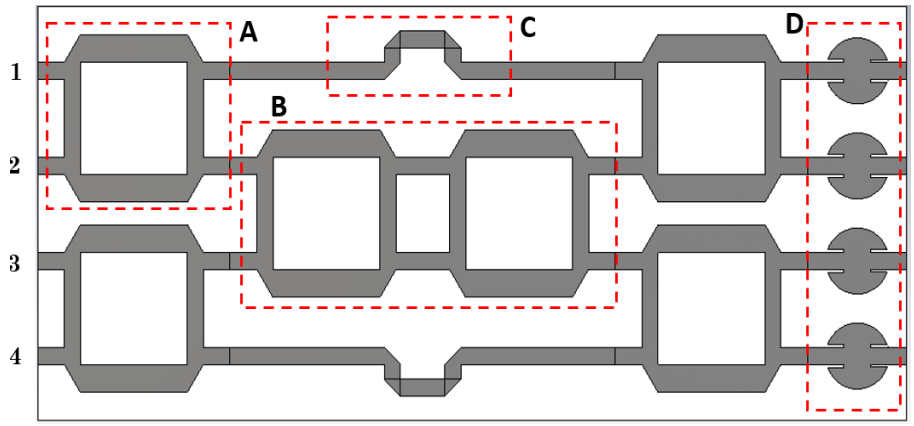

Figure 4.15. Circular patch array with Buttler beamforming network

At the central frequency of $f_c = 77\ GHz$ the angular directions of the main beam by switching between ports 1 to 4 are summarized in table 4-7.

Table 4-7. Angular directions of the main beam at 77 GHz

Port Number	**1**	**2**	**3**	**4**
Angle of the main beam	$+149^{\circ}$	$+14^{\circ}$	-14°	-149°

Based on table 4-8, we can easily see that by excitation of any of the ports 1 to 4 at a given time, we could have beam scanning with 2 right angles and two left angles. The range-Doppler performance of the circular patch array using Buttler beamformer is shown on figure 4-16. The red elliptic shapes show the target returns. The gain of the antenna system is relatively low. As was the case with the inset-fed patch antenna, we believe by doing some antenna tuning and optimization in the designed array, we could possibly improve the gain. In this case, the radar returns have power of -30dB to -35dB which are still detectable against the background noise with -80dB power.

Table 4.8. Propagation Patterns of the circular patch array with Buttler beamforming network

Frequency (GHz)	Propagation pattern (plane $\boldsymbol{\varphi} = \mathbf{0}^{\circ}$)			
	Port 1	Port 2	Port 3	Port 4
76.5	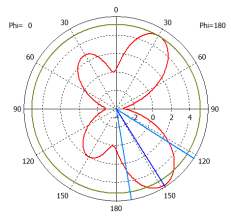	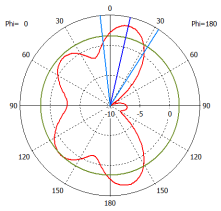	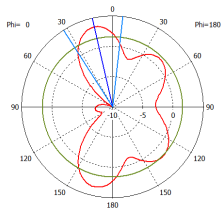	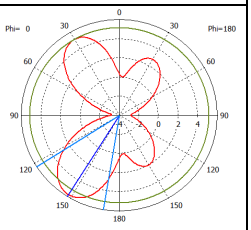
77	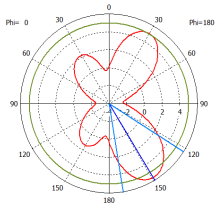	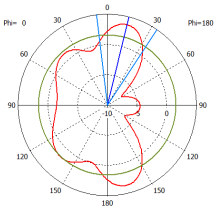	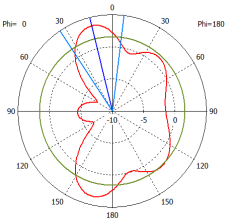	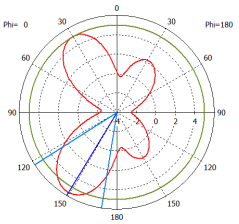
77.5	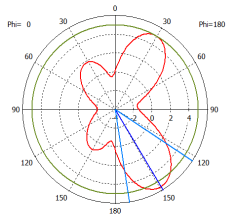	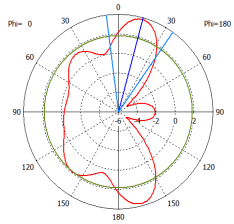	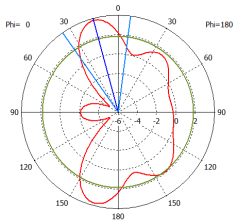	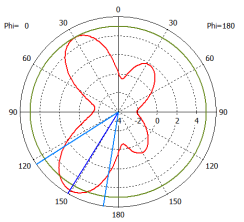
78	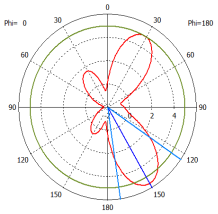	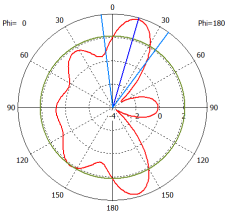	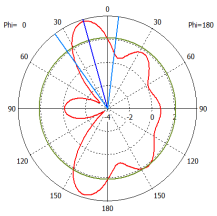	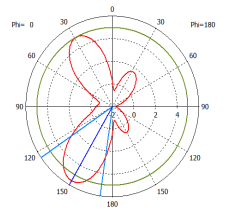

Tables 4.9, 4.10 and 4.11 summarize the range-Doppler data of the three antenna systems in the proposed FMCW radar system. The first four columns in each table correspondingly show the real velocity (V_{real}), the real range (R_{real}), the real relative velocity of the target to the radar (ΔV_{real}) and the real relative range of the target to the radar (ΔR_{real}) and these

are fixed values in all three tables. The last two columns show the estimated relative velocity and the estimated relative range of each target.

As was the case with the inset-fed patch antenna, we believe by doing some antenna tuning and optimization in the designed array, we could possibly improve the gain. In this case, the radar returns have power of -30dB to -35dB which are still detectable against the background noise with -80dB power.

Table 4.9. Range-Doppler results of circular patch array with Buttler Beamformer

Obj\ Par.	V_{real}	R_{real}	ΔV_{real}	ΔR_{real}	ΔV_{est}	ΔR_{est}
Truck	129.99	65	+32.79	65	+32.10	63.07
Car	59.97	65	-37.23	65	-38.52	63.07
Motorcycle	126	45	28.8	45	+29.8	44.52
Bike	46.8	20	-50.4	20	-57.78	18.55

Table 4.10. Range-Doppler results of the Inset-fed patch array

Obj\ Par.	V_{real}	R_{real}	ΔV_{real}	ΔR_{real}	ΔV_{est}	ΔR_{est}
Truck	129.99	65	+32.79	65	+29.96	59.36
Car	59.97	65	-37.23	65	-49.22	59.36
Motorcycle	126	45	28.8	45	+29.96	40.81
Bike	46.8	20	-50.4	20	-53.5	22.26

Table 4.11. Range-Doppler results of the Comb-line leaky wave antenna

Obj\ Par.	V_{real}	R_{real}	ΔV_{real}	ΔR_{real}	ΔV_{est}	ΔR_{est}
Truck	129.99	65	+32.79	65	+32.10	63.07
Car	59.97	65	-37.23	65	-40.66	63.07
Motorcycle	126	45	28.8	45	+27.82	44.52
Bike	46.8	20	-50.4	20	-55.64	20.77

In addition to the tables 4.9, 4.10 and 4.11, the range-Doppler results of the three proposed antenna systems have been shown as graphs on figure 4.16. On this figure, the horizontal axis is δV which is the speed of a target relative to the speed of radar and the vertical axis is showing δR which is the position of a target relative to the position of radar. There are 4 curves in the figure. The blue curve is the reference curve, the red, green and black curves show the range-Doppler responses of circular patch array with Buttler beamforming network, the inset-fed patch array and the comb-line leaky wave antenna correspondingly. The pink circles show the range-Doppler margin of 3 targets. We can see that the Buttler beamformer's performance is the best but at the cost of more complexity in design. The comb-line leaky wave antenna has a decent range-Doppler performance and is showing a better margin than the inset-fed patch array for target 2. The comparison of the range-Doppler performances of the comb-line leaky wave antenna in FMCW radar system proves that this cheap antenna solution can replace the state-of-the-art antenna arrays and the simple structure of this antenna could reduce the cost of fabrication in the automotive industry.

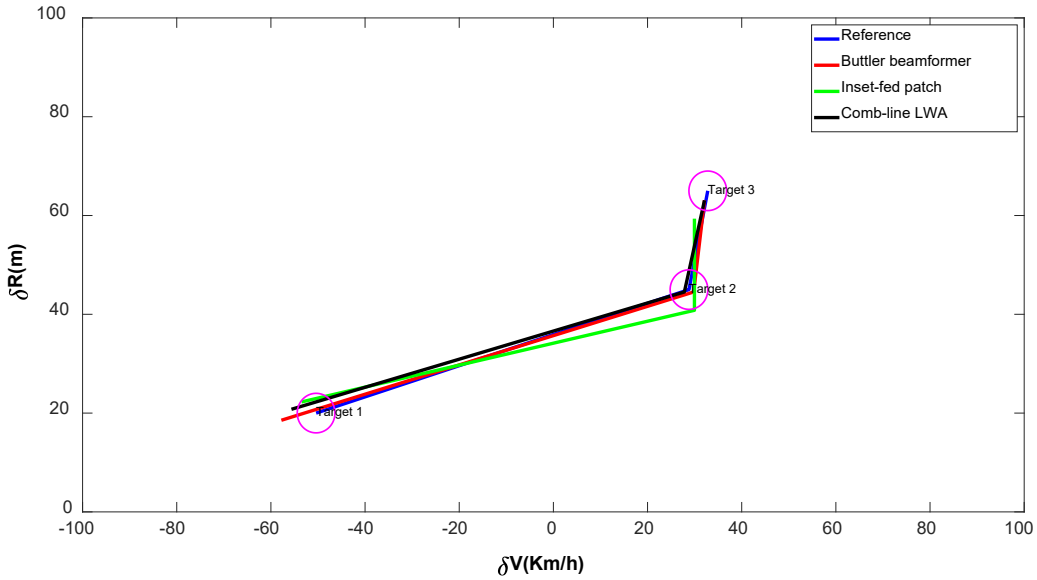

Fig 4.16. Range-Doppler performance of the Buttler beamformer network, Inset-fed patch array & comb-line leaky wave antenna

4.6 Conclusion

In this work, we proposed a comb-line leaky wave antenna that is applicable to a multi-target automotive FMCW radar system. The proposed antenna is simple in structure, cheap in manufacture and also the range-Doppler results show that the applied antenna could offer a good solution for automotive industry. Also, two antenna array structures were proposed in section V, including the inset-fed patch antenna array as well as circular patch array controlled with a Buttler beamforming network. Comparing the range-Doppler results of all 3 cases prove that the proposed leaky wave antenna can actually be a substitute for generic antenna arrays with complex beamforming network that are typically used in automotive radars. Although, antenna arrays may offer higher precision in range-Doppler measurements but the authors believe that the functionality of the proposed leaky wave antenna results in acceptable range and velocity margins for road safety and automotive

applications. Observing range-Doppler maps on figures 8 to 10 show that ghost targets cannot be avoided in FMCW radars once we use triangular chirp. The authors believe that the negative ramp of the triangular chirp somehow creates images of the main targets in a symmetrical fashion. Under section IV we actually discussed and categorized and discussed the ghost targets of type I and type II. Ghost targets of type II can be easily ignored because their range and velocity values are beyond real automotive scenarios. But ghost targets of type I, emerge exactly within the same velocity values of the genuine target returns and have the negated range values of real targets, which make them significant to detect and suppress. The fix was using a sawtooth chirp to cancel out the effect of the negative ramp in the triangular chirp.

4.7 References

[1] https://www.nhtsa.gov/

[2] Jankiraman, Mohinder. FMCW Radar Design. Artech House, 2018.

[3] Kärnfelt, Camilla, et al. "77 GHz ACC radar simulation platform." 2009 9th International Conference on Intelligent Transport Systems Telecommunications, (ITST). IEEE, 2009.

[4] Lin, Jau-Jr, et al. "Design of an FMCW radar baseband signal processing system for automotive application." SpringerPlus 5.1 (2016): 1-16.

[5] Steeg, Matthias, Asmaa Al Assad, and Andreas Stöhr. "Simultaneous DoA estimation and ranging of multiple objects using an FMCW radar with 60 GHz leaky-wave antennas." 2018 43rd International Conference on Infrared, Millimeter, and Terahertz Waves (IRMMW-THz). IEEE, 2018.

[6] Yang, Shang-Te, and Hao Ling. "Application of a microstrip leaky wave antenna for range–azimuth tracking of humans." IEEE Geoscience and Remote Sensing Letters 10.6 (2013): 1384-1388.

[7] Ammen, Daiki, et al. "A Ghost Target Suppression Technique using Interference Replica for Automotive FMCW Radars." 2020 IEEE Radar Conference (RadarConf20). IEEE, 2020.

[8] Gross, Frank B. Frontiers in antennas: next generation design & engineering. McGraw-Hill Education, 2011.

[9] Hyneman, R. "Closely-spaced transverse slots in rectangular waveguide." IRE Transactions on Antennas and Propagation 7.4 (1959): 335-342.

[10] Brillouin, L. "Wave Propagation in Periodic Structures, DoverPublications." (2003).

[11] Rohling, H. and M. Meinecke. Waveform Design Principle for Automotive Radar Systems, Proceedings of CIE International Conference on Radar, 2001.

5 Conclusion and Future work

We set 2 goals for this work. The first goal was to propose and design one-dimensional and two-dimensional leaky wave antennas that could be used as biomedical application for treatment of hyperthermia. In this process, we started with designing the simplest possible slotted LWA with working frequency of 13.8 GHz to 15.2 GHz. We found the optimal excitation pulse envelope which turned out to be trapezoidal envelope and for the sake of simulation, we defined a bio-tissue which was located in proximity of a few millimeters from the antenna and then the electromagnetic as well as the thermal behavior of this structure was studied. For this design the thermal results showed high temperatures but to make the scenario more realistic we decreased the pulse excitation time to about a few minutes. That is to avoid exposing the healthy cells that surround the cancerous cells, to too much heat for a considerable time. heat that would lead to damage of those cells. In another design process, we came up with three 2D leaky wave antennas such as mushroom-typed LWA, periodically-slotted leaky wave antenna, belt-shaped leaky wave antenna. The type of hyperthermia tool could differ depending on what depth the tumor is located, at which body organ and also what beam geometry could be more efficient for that specific tumor. Based on these factors, as recently mentioned in chapter III, hyperthermia is of 2 types of superficial hyperthermia (SHT) and deep hyperthermia (DHT). According to the ISM bands, one of the most typical frequencies for biomedical devices is 2.45 GHz. Our design in the 1D leaky wave antenna is focused outside the ISM band while in our 2D leaky wave antenna designs we have used the central frequency of 2.45 GHz. The depth of penetration is smaller for higher frequencies while for lower frequencies this depth is bigger. That would give us the opportunity to use SHT or DHT depending on the position of a tumor. In addition to that our proposed ring-shaped LWA is actually a conformal antenna that could be specifically used for neck or head tumors. In each design we have compared the results of specific absorption ratio (SAR) with the American or European SAR limits. For example, in US the permitted SAR value for treatment devices is limited to $1.6\ W/Kg$ and we have discussed the evaluation of such results in the same chapter.

Additionally, we proposed a multi-target FMCW radar system that uses comb-line LWA as beamformer. The proposed antenna system offers a decent angle coverage that makes it suitable for automotive applications. We also designed 2 antenna arrays which were inset-fed patch antenna and circular patch antenna array with Buttler matrix as beamformer that provided 2 right-handed angles and 2 left-handed angles. For all the cases, the range-Doppler maps were compared together and we observed that a single leaky wave antenna could offer a decent beam scanning and a cheap solution compared to the state-of-the-art radar solutions. Chapter IV discusses the results in more depth.

5.1 Future work

We believe that 2D leaky wave antennas could give more beam control that makes them good candidates for hyperthermia therapy. Since by switching between frequencies we can get different beam geometry, the author suggests that there is room for further development of such biomedical antennas working at ISM bands. To continue this research, antenna prototypes could be built and material with similar partitivities to body tissues could mimic the real tissues. The antennas could be conformal which means that they could be fit to the shape of the body organ that needs thermal treatment such as the example of the ring-shaped LWA for neck tumors. Then the radiation effect for temperature rise could be measured and further studied to better understand the pros and cons of the proposed designs.

There could be a huge market for FMCW automotive radar systems and to achieve that more antenna designs and more efficient signal processing and smart ghost suppression algorithms could be tested to find the cheapest possible solutions. Only that would guarantee a considerable improvement in the road safety both for drivers and pedestrians.

A Return Loss Data Extraction from CST

```
% This code translates the .txt file (ASCII) of the S-Plot in CST into
% the struct and finally extracts the numerical data of this struct for
%plotting S11, then tracks the minima of the periodic return data, and
%final calculates the frequency difference between the minima points %

clear all
close all
%A = importdata('\\homes.mtu.edu\home\Desktop\radar\S11.txt');
%A = importdata('\\homes.mtu.edu\home\Desktop\radar\asymmetric_Combline.txt');
A = importdata('\\homes.mtu.edu\home\Desktop\radar\asymmetrical_typ2_combline.txt');

%B= importdata('\\homes.mtu.edu\home\Desktop\radar\S11_Matched.txt');
% B=cell2mat(struct2cell(A.data));
% C= cell2mat((A.data));
value_A = struct2cell(A(1));
S11_data_A=cell2mat(value_A(1,1));
f1=S11_data_A(:,1);
Gain1=S11_data_A(:,2);


% value_B = struct2cell(B(1));
% S11_data_B=cell2mat(value_B(1,1));
% f2=S11_data_B(:,1);
% Gain2=S11_data_B(:,2);
plot(f1,Gain1,'LineWidth',3)
set(gca,'FontSize',20)
% hold on
% plot(f2,Gain2,'LineWidth',3)

set(gca,'FontSize',20)
xlabel('f(GHz)')
ylabel('Gain(dB)')
legend({'Return Loss for Unmatched Antenna','Return Loss for Matched
Antenna'},'FontSize',14)


Pe=0.008; % period of the combline structure %
er=9.2;
f0=77*10^9;
c=3*10^8;
Beta0=(2*pi*f0)/c;
Beta_n=[];

for n=1:10
```

```
Beta = Beta0 + (2*n*pi)/Pe;
Beta_n = [Beta_n  Beta ];
end
Vp=c/sqrt(er);
f_p = (Beta_n*Vp)/(2*pi);  %candidate resonance frequencies %

%%% Find Minima %%%

[P, index]=findpeaks(-Gain1);
freq=f1(index)
minima=[freq';-P'];
Delta_f=diff(freq)
% S = sparameters('\\homes.mtu.edu\home\Desktop\Match.s1p');
% disp(S)
% rfplot(S)
```

B SAR Image Processing MATLAB Code

```
%% SAR Image Processing %%
%% The code reads the SAR image and calculates the geometry and the affected
%% area by hyperthermia by counting the number of Red pixels, Red pixels illustrate
%% The areas with highest heat absorption %%
%% Masoud Sarabi, 24 Dec. 2020 %%

%%Load image%%
clear all
close all
rgb = imread ('\\homes.mtu.edu\home\Desktop\filtered SAR maps\2D periodically slotted
leaky wave antenna\2.45GHz.png');

% Tissue area in mm-squared %
Tissue_area = (159.7^2);
%Tissue_area=76*pi*60;

[rows columns numberOfColorChannels] = size(rgb);
% Number of all pixels in image %
NumberOfPixels = rows*columns;

figure(1)

imshow(rgb)
%%Find red points %%
%% NOTE: the rgb (:, : ,2) should be chosen carefully, it could lead to so
%% much smearing if too high or detected area smaller than reality if too low %

redPixels = rgb(:,:,1)>=130 & rgb(:,:,2)<=155 & rgb(:,:,3)<=110;
percentRed = 100*(sum(sum(redPixels))/(size(rgb,1)*size(rgb,2)));
 fprintf('Image has %d red pixels\n',sum(sum(redPixels)))
 fprintf('Image is %.2f percent red\n',percentRed)


%% Highlight red on image %%
rgbRed = uint8(cat(3,redPixels,redPixels,redPixels)).*rgb;
figure(2)
imshow(rgbRed)

% Calculation of the Hyperthermia area in mm-squared %
Hyperthermia_area=(nnz(redPixels)/NumberOfPixels)* Tissue_area;
fprintf('Hyperthermia area in mm-squared is %d \n',Hyperthermia_area)
```

C MATLAB Code for FMCW RADAR

```
% Multi-Target FMCW RADAR %
% MASOUD SARABI %
% Michigan Technological University %
% Electrical & Computer Engineering Department %
% Summer 2019 %

% clear all;
% close all;

fc=[72e9 77e9 79e9];   % Operating frequency vector of RADAR %
c=3e8;
lambda=c./fc;

% Defining (maximum) range, while sweeptime should be 5 to 6 times the round
% trip time %

range = 200;
M = 5.5;
tm = M*range2time(range,c);   %Sweeptime, range2time(Range,V) actually uses the
formula t=(2R)/V %

range_res = 1;   % was originally 1 %
bw = range2bw(range_res,c);
sweep_slope = bw/tm;   % there are 2 slopes for triangular wave
%sweep_slope = -bw/tm;

% target(s) speed in m/s %

Vm1=130*(1000/3600);  %Vm Km/h %
```

```
Vm2=110*(1000/3600);
Vm3=90*(1000/3600);

% Because of triangular sweep we should have two beat frequencies the
% positive fb  and the negative fb ???

% fb_positive = range2beat(range,sweep_slope,c);
% fb_negative = range2beat(range,-sweep_slope,c);

% fb_positive=2*bw*range/(c*tm)-(2*Vm*fc/c);
% fb_negative=2*bw*range/(c*tm)+(2*Vm*fc/c);

%1st target %
fb_positive1=2*bw*range/(c*tm)+(2*Vm1*fc/c);
fb_negative1=2*bw*range/(c*tm)-(2*Vm1*fc/c);

%2nd target %
fb_positive2=2*bw*range/(c*tm)+(2*Vm2*fc/c);
fb_negative2=2*bw*range/(c*tm)-(2*Vm2*fc/c);

%3rd target %
fb_positive3=2*bw*range/(c*tm)+(2*Vm3*fc/c);
fb_negative3=2*bw*range/(c*tm)-(2*Vm3*fc/c);

% Doppler frequencies %
fd1=speed2dop(2*Vm1,min(lambda));   % Using fd=(2*Vm*cos(theta))/lambda %  %
Min of lambda vector is calculated %
fd2=speed2dop(2*Vm2,min(lambda));
fd3=speed2dop(2*Vm3,min(lambda));
```

```
fb_doppler_up1 = fb_positive1+fd1;
fb_doppler_down1 = fb_negative1+fd1;

fb_doppler_up2 = fb_positive2+fd2;
fb_doppler_down2 = fb_negative2+fd2;

fb_doppler_up3 = fb_positive3+fd3;
fb_doppler_down3 = fb_negative3+fd3;

 %%%%%%%%%%%%%%%%%%%%
fs1=max(2*fb_doppler_up1,bw);
fs2=max(2*fb_doppler_down1,bw);
fs3=max(2*fb_doppler_up2,bw);
fs4=max(2*fb_doppler_down2,bw);
fs5=max(2*fb_doppler_up3,bw);
fs6=max(2*fb_doppler_down3,bw);

fs_m=[fs1 fs2 fs3 fs4 fs5 fs6];
fs=max(fs_m)

% fs_m1=max(fs1,fs2);
% fs_m2=max(fs3,fs4);
% fs_m3=max(fs5,fs6);
% fs=max(fs_m1,fs_m2);
%fs=min(fs1,fs2);

%%%%%%%%%%%%%%

Nsweep = 2
```

```
% Defining triangular sweep with FMCWWaveform fnc. %

%waveform=
phased.FMCWWaveform('SweepTime',tm,'SweepDirection','Triangle','SweepBandwidth'
,bw, 'SampleRate',fs);%

%  waveform = phased.FMCWWaveform('SweepTime',tm, 'SweepDirection','Triangle',
'NumSweeps',Nsweep);

%  waveform = phased.FMCWWaveform('SweepTime',tm,...
% 'SampleRate',fs,'SweepDirection','Triangle',...
%  'NumSweeps',4);

% The following FMCW definition worked properly %
%waveform = phased.FMCWWaveform('SweepTime',tm,...
%     'SweepBandwidth',bw,'SweepDirection','Triangle',...
%     'SweepInterval','Symmetric','SampleRate',fs,...
%     'OutputFormat','Sweeps','NumSweeps',Nsweep);


waveform = phased.FMCWWaveform('SweepTime',tm,'SweepBandwidth',bw,...
   'SampleRate',fs,'SweepDirection','Triangle',...
   'NumSweeps',Nsweep);

%      st = [tm/2 tm/2];
%      bandwidth=[bw bw];
%     waveform = phased.FMCWWaveform('SweepTime',st,...
%     'SweepBandwidth',bandwidth,'SweepDirection','Triangle',...
%     'SweepInterval','Symmetric','SampleRate',fs,...
```

```
%     'NumSweeps',Nsweep);

%     sig = waveform();
sig = step(waveform);

[Line Col] = size(sig);
g=linspace(0,tm-1/fs,Line);

%    x=0:1/(6*fs):tm-1/fs;

subplot(211);
%plot(0:1/(fs):tm-1/fs,real(sig));

plot(g,real(sig));
xlabel('Time (s)'); ylabel('Amplitude (v)');
title('FMCW signal'); axis tight;

subplot (212);
spectrogram(sig,32,16,32,2*fs,'yaxis'); %we used 2*fs as sampling rate otherwise the
spectrogram and waveform time durations wouldn't match %
%spectrogram(sig, windowlength,noverlap,nfft,sFMCW.SampleRate,'yaxis')
Title ('FMCW signal spectrogram');

% 2nd Method for plotting SPECTROGRAM %
%
% [Line Col] = size(sig);
% g=linspace (0,tm-1/fs, Line);
% subplot(211);
% plot(g,real(sig));
% xlabel ('Time (s)'); ylabel ('Amplitude (v)');
```

```
% title('FMCW signal'); axis tight;
% subplot(212);
% %[S,F,T] = spectrogram(sig,32,16,32,waveform.SampleRate);
% [S,F,T] = spectrogram(sig,32,16,32,fs,'yaxis');
% image(T,fftshift(F),fftshift(mag2db(abs(S))))
% xlabel ('Time (sec)')
% ylabel ('Frequency (Hz)')
% waveform.PRF = 1/tm;
% waveform.SampleRate = fs;

% AMBIGUITY FUNCTION %
[mag,delay,doppler]= ambgfun(sig,waveform.SampleRate,1./(2*waveform.SweepTime));

[afmag_lfm,delay_lfm,doppler_lfm] = ambgfun(sig,...
waveform.SampleRate,waveform.PRF);

% The waveform.PRF part needs to be defined in a different way %

size(sig)
PRF=1/tm;          % PRF= Pulse Repetition Frequency %
fs_amb=101*PRF;
 % Previously this frequency was the same as fs which was 150MHz, but we changed it
to lower value and here we go! one step forward, because initially we couldn't get the
"ambgfun" to work %

[mag,delay,doppler] = ambgfun(sig',fs_amb,PRF);

figure
surf(delay*1e6,doppler/1e3,mag, 'LineStyle','none')
axis tight
```

```
grid on
view([140,35])
colorbar
xlabel ('Delay \tau (\mus)')
ylabel ('Doppler f_d (kHz)')
title ('Linear FM Pulse Waveform Ambiguity Function')

% 2D countour plots %
figure
contour(delay,doppler,mag)

%PLOT Doppler/Delay CUTS OF AMBIGUITY FUNCTION %

bandwidth(sig)
figure
ambgfun(sig',fs_amb,PRF,'Cut','Doppler');
figure
ambgfun(sig',fs_amb,PRF,'Cut','Delay');

% TARGET(S) MODEL %
% To model the target, distance, velocity and RCS would be needed %

obj_distance1 = 70;
obj_distance2 = 40;
obj_distance3 = 50;
%
obj_speed1=50*(1000/3600);
obj_speed2=50*(1000/3600);
obj_speed3=50*(1000/3600);
% obj_speed1=130*(1000/3600);
```

```
% obj_speed2=110*(1000/3600);
% obj_speed3=90*(1000/3600);

% RCS of targets %
obj_rcs1=db2pow(min(10*log10(obj_distance1) +5,20));  % Car %

obj_rcs2=2*db2pow(min(20*log10(obj_distance2) +5,20)); % Truck %

obj_rcs3=1.5*db2pow(min(20*log10(obj_distance3) +5,20)); % Motorcycle %

% Target #1 %
obj_target1_1 = phased.RadarTarget('MeanRCS',obj_rcs1,'PropagationSpeed',c,...
   'OperatingFrequency', fc(1));

obj_target1_2 = phased.RadarTarget('MeanRCS',obj_rcs1,'PropagationSpeed',c,...
   'OperatingFrequency', fc(2));

obj_target1_3 = phased.RadarTarget('MeanRCS',obj_rcs1,'PropagationSpeed',c,...
   'OperatingFrequency',fc(3));

% Target #2 %
obj_target2_1 = phased.RadarTarget('MeanRCS',obj_rcs2,'PropagationSpeed',c,...
   'OperatingFrequency',fc(1));

obj_target2_2 = phased.RadarTarget('MeanRCS',obj_rcs2,'PropagationSpeed',c,...
   'OperatingFrequency',fc(2));

obj_target2_3 = phased.RadarTarget('MeanRCS',obj_rcs2,'PropagationSpeed',c,...
   'OperatingFrequency',fc(3));
% Target #3 %
```

```
obj_target3_1 = phased.RadarTarget('MeanRCS',obj_rcs3,'PropagationSpeed',c,...
   'OperatingFrequency',fc(1));

obj_target3_2 = phased.RadarTarget('MeanRCS',obj_rcs3,'PropagationSpeed',c,...
   'OperatingFrequency',fc(2));

obj_target3_3 = phased.RadarTarget('MeanRCS',obj_rcs3,'PropagationSpeed',c,...
   'OperatingFrequency',fc(3));

%% reflection %%   % e.g. If we have 3 targets, using 3 scanning frequencies, gives back
9 reflections overall %
ref1_f1=step(obj_target1_1,sig);
ref1_f2=step(obj_target1_2,sig);
ref1_f3=step(obj_target1_3,sig);

ref2_f1=step(obj_target2_1,sig);
ref2_f2=step(obj_target2_2,sig);
ref2_f3=step(obj_target2_3,sig);

ref3_f1=step(obj_target3_1,sig);
ref3_f2=step(obj_target3_2,sig);
ref3_f3=step(obj_target3_3,sig);

%%%%%%%% Initial target properties , position,... %%%%%%%%
obj_motion1 = phased.Platform('InitialPosition',[obj_distance1;0;3],...
   'Velocity',[obj_speed1;0;0]);

obj_motion2 = phased.Platform('InitialPosition',[obj_distance2;0;4],...
   'Velocity',[obj_speed2;0;0]);
```

```
obj_motion3 = phased.Platform('InitialPosition',[obj_distance3;0;6],...
    'Velocity',[obj_speed3;0;0]);

%%%%%%%%%%%%%%%%%%%%%%%%%%%%%%%%%%%%%%%%%
% Channel Model %
% In this code we consider the signal transmission in free space %
channel_1 = phased.FreeSpace('PropagationSpeed',c,...
    'OperatingFrequency',fc(1),'SampleRate',fs,'TwoWayPropagation',true);   % Channel
behaves differently for different frequencies, here's the channel for first frequency%

channel_2 = phased.FreeSpace('PropagationSpeed',c,...
    'OperatingFrequency',fc(2),'SampleRate',fs,'TwoWayPropagation',true);

channel_3 = phased.FreeSpace('PropagationSpeed',c,...
    'OperatingFrequency',fc(3),'SampleRate',fs,'TwoWayPropagation',true);


% RADAR SYSTEM %
% Most definitely, aperture and gain is not constant for LWA in different
% frequencies and we must integrate that antenna soon, especially because
% they are frequency scanning antennas. Here we just consider an ideal
% isotropic antenna for simplicity %

% Periodic/Metamaterial Leaky Wave Antenna Design %

% Isotropic Antenna or later on LWAs %
% Tx_gain = 15; % Tx Amplifier gain in dB
%Rx_gain = 9;  % Rx amplifier gain in dB
```

```
% Realistic antenna %
Tx_gain = [12 17 15];
Rx_gain = [6 9 8];
% TX gain should be a vector too due to reciprocity, later on we would consider
                % the arithmetic average of these numbers %

% ant_aperture = 6.06e-4;
% Aperture for isotropic antenna in square meter
%ant_gain = aperture2gain(ant_aperture,lambda);  % This MUST be one of the
                                                 % points of novelties for this radar project,because
                                                 % a CRLH leaky wave
                                                 % antenna is to be used in
                                                 % the radar system and
                                                 % this could affect
                                                 % performance and cost of
                                                 % the whole system.


ant_aperture = [4.06e-4 6.06e-4 5.06e-4];

Gain_dB=10*log10((4*pi*ant_aperture)./(lambda.^2));   % Calculation of the antenna
gain in dB using aperture %

tx_power=db2pow(5)*1e-3;
tx_gain=Tx_gain+Gain_dB;

rx_gain=Rx_gain+Gain_dB; % Receiver gain in dB %
rx_NF=5; % Noise figure in dB %
```

```
transmitter_1 = phased.Transmitter('PeakPower',tx_power,'Gain',tx_gain(1));
transmitter_2 = phased.Transmitter('PeakPower',tx_power,'Gain',tx_gain(2));
transmitter_3 = phased.Transmitter('PeakPower',tx_power,'Gain',tx_gain(3));

%receiver = phased.ReceiverPreamp('Gain',rx_gain(1),'NoiseFigure',rx_NF,...    %
   %'SampleRate',fs);    % What type of receiver is this ? %

receiver = phased.ReceiverPreamp('Gain',sum(rx_gain)/3,'NoiseFigure',rx_NF,
'SampleRate',fs);  % took the average gain %

%% Radar Motion %

radar_speed = 50*1000/3600;
radarmotion = phased.Platform('InitialPosition',[0;0;3],...
   'Velocity',[radar_speed;0;0]);

% Demostration on spectrum analyzer %

specanalyzer = dsp.SpectrumAnalyzer('SampleRate',fs,...
   'PlotAsTwoSidedSpectrum',true,...
   'Title','Spectrum for received and dechirped signal',...
   'ShowLegend',true);

%%%%% Pulse Integration %%%%%

rng (2012);
N = 64;
% Number of sweeps. Keep in mind that with minimum of 2 sweeps
% we are able to distinguish between the doppler frequency (fd) and beat
% frequency (fb)
```

```
xr = complex(zeros(waveform.SampleRate*waveform.SweepTime,N));
% waveform.SampleRate*waveform.SweepTime is time-bandwidth product,
% the higher it is, the better would be the resolution %

 for m=1:N
    % Radar's and target's speed-position update %
    [radar_position,radar_velocity] = radarmotion(waveform.SweepTime);

    [target_position1,target_velocity1]=obj_motion1(waveform.SweepTime);
    [target_position2,target_velocity2]=obj_motion2(waveform.SweepTime);
    [target_position3,target_velocity3]=obj_motion3(waveform.SweepTime);
    % Transmission of FMCW waveform

    sig = waveform();
    tx_sig_1 = transmitter_1(sig);
    tx_sig_2 = transmitter_2(sig);
    tx_sig_3 = transmitter_3(sig);

    % propagation of signal and reflection off the target %
    tx_sig1 =
channel_1(tx_sig_1,radar_position,target_position1,radar_velocity,target_velocity1);
    tx_sig2 =
channel_2(tx_sig_2,radar_position,target_position2,radar_velocity,target_velocity2);
    tx_sig3 =
channel_3(tx_sig_3,radar_position,target_position3,radar_velocity,target_velocity3);


    tx_sig1_1 = obj_target1_1(tx_sig1);
    tx_sig1_2 = obj_target1_2(tx_sig1);
    tx_sig1_3 = obj_target1_3(tx_sig1);
```

```
tx_sig2_1 = obj_target2_1(tx_sig2);
tx_sig2_2 = obj_target2_2(tx_sig2);
tx_sig2_3 = obj_target2_3(tx_sig2);

tx_sig3_1 = obj_target3_1(tx_sig3);
tx_sig3_2 = obj_target3_2(tx_sig3);
tx_sig3_3 = obj_target3_3(tx_sig3);

% Dechirping of the received radar return, 2 ways are considerable :1) addition of two signals and then applying the receiver 2) %applying the receiver to each signal and then addition %

    %%% Method 1 %%%%
    tx_sig_sum_f1=receiver(tx_sig1_1+tx_sig2_1+tx_sig3_1);
    tx_sig_sum_f2=receiver(tx_sig1_2+tx_sig2_2+tx_sig3_2);
    tx_sig_sum_f3=receiver(tx_sig1_3+tx_sig2_3+tx_sig3_3);


    %%% addition of echoes %%%%%

    dechirped_signal_f1 = dechirp(tx_sig_sum_f1 ,sig);
    dechirped_signal_f2 = dechirp(tx_sig_sum_f2 ,sig);
    dechirped_signal_f3 = dechirp(tx_sig_sum_f3 ,sig);


    [row_f1 column_f1]=size(dechirped_signal_f1)
    [row_f2 column_f2]=size(dechirped_signal_f2)
    [row_f3 column_f3]=size(dechirped_signal_f3)
```

```
    %Visualize the spectrum %
  specanalyzer([tx_sig_sum_f1 dechirped_signal_f1]); % output is sinc^2 fnc. which is the fourier transform of a triangular pulse %
  specanalyzer([tx_sig_sum_f2 dechirped_signal_f2]);
  specanalyzer([tx_sig_sum_f3 dechirped_signal_f3]);


    xr_f1(1:row_f1,m) = dechirped_signal_f1;    % Problem solved : the xr and dechirped_signal didn't match in size.
    xr_f2(1:row_f2,m) = dechirped_signal_f2;
    xr_f3(1:row_f3,m) = dechirped_signal_f3;
 end

%size(tx_sig)
%size(dechirped_signal)

% Extract the Doppler response

rngdopresp1 = phased.RangeDopplerResponse('PropagationSpeed',c,...
   'DopplerOutput','Speed','OperatingFrequency',fc(1),'SampleRate',fs,...
   'RangeMethod','FFT','SweepSlope',sweep_slope,...
   'RangeFFTLengthSource','Property','RangeFFTLength',2048,...
   'DopplerFFTLengthSource','Property','DopplerFFTLength',256);

rngdopresp2 = phased.RangeDopplerResponse('PropagationSpeed',c,...
   'DopplerOutput','Speed','OperatingFrequency',fc(2),'SampleRate',fs,...
   'RangeMethod','FFT','SweepSlope',sweep_slope,...
   'RangeFFTLengthSource','Property','RangeFFTLength',2048,...
   'DopplerFFTLengthSource','Property','DopplerFFTLength',256);
```

```
rngdopresp3 = phased.RangeDopplerResponse('PropagationSpeed',c,...
    'DopplerOutput','Speed','OperatingFrequency',fc(3),'SampleRate',fs,...
    'RangeMethod','FFT','SweepSlope',sweep_slope,...
    'RangeFFTLengthSource','Property','RangeFFTLength',2048,...
    'DopplerFFTLengthSource','Property','DopplerFFTLength',256);

V_m=[Vm1,Vm2,Vm3];

% plotResponse(rngdopresp1, xr_f1);  %%% ?????? %%%
 plotResponse(rngdopresp2, xr_f2);
% plotResponse(rngdopresp3, xr_f3);

axis([-max(V_m) max(V_m) 0 range])
clim = caxis;



a1=min(fb_doppler_up1,fb_doppler_down1)
a2=min(fb_doppler_up2,fb_doppler_down2)
a3=min(fb_doppler_up3,fb_doppler_down3)

a=[a1 a2 a3];

Dn = fix(fs/(min(a)));
% Here we pick the smallest Doppler frequency to get the maximal decimated
% sampling frequency fs-d %

for m = size(xr_f1,2):-1:1
    xr_f1_d(:,m) = decimate(xr_f1(:,m),Dn,'FIR');
    xr_f2_d(:,m) = decimate(xr_f2(:,m),Dn,'FIR');
```

```
    xr_f3_d(:,m) = decimate(xr_f3(:,m),Dn,'FIR');
end
fs_d = fs/Dn;


fb_rng_1 = rootmusic(pulsint(xr_f1_d,'coherent'),1,fs_d);
fb_rng_2 = rootmusic(pulsint(xr_f2_d,'coherent'),1,fs_d);
fb_rng_3 = rootmusic(pulsint(xr_f3_d,'coherent'),1,fs_d);


rng_est_1 = beat2range(fb_rng_1,sweep_slope,c)
rng_est_2 = beat2range(fb_rng_2,sweep_slope,c)
rng_est_3 = beat2range(fb_rng_3,sweep_slope,c)

%%%%%%%%%%%%%%%%%%%%%%%%%%%%%%%%%%%%

peak_loc_1 = val2ind(rng_est_1,c/(fs_d*2));
peak_loc_2 = val2ind(rng_est_2,c/(fs_d*2));
peak_loc_3 = val2ind(rng_est_3,c/(fs_d*2));

fd_1 = -rootmusic(xr_f1_d(peak_loc_1,:),1,1/tm);
fd_2 = -rootmusic(xr_f2_d(peak_loc_2,:),1,1/tm);
fd_3 = -rootmusic(xr_f3_d(peak_loc_3,:),1,1/tm);

%%%%%%%%%%%%%%%%%%%%%%%%%%%%%%%%%%%%


v_est_1_1 = dop2speed(fd_1,lambda(1))/2
v_est_1_2 = dop2speed(fd_1,lambda(2))/2
v_est_1_3 = dop2speed(fd_1,lambda(3))/2
```

```
v_est_2_1 = dop2speed(fd_2,lambda(1))/2
v_est_2_2 = dop2speed(fd_2,lambda(2))/2
v_est_2_3 = dop2speed(fd_2,lambda(3))/2

v_est_3_1 = dop2speed(fd_3,lambda(1))/2
v_est_3_2 = dop2speed(fd_3,lambda(2))/2
v_est_3_3 = dop2speed(fd_3,lambda(3))/2;

delta_R_1=rdcoupling(fd_1,sweep_slope,c)
delta_R_2=rdcoupling(fd_2,sweep_slope,c)
delta_R_3=rdcoupling(fd_3,sweep_slope,c)

waveform_updated=clone(waveform);
release(waveform_updated);
tm = 2e-3;
waveform_updated.SweepTime = tm;
sweep_slope = bw/tm;

%%%%%%%%%%%%%%%%%%%%%%%%%%%%

delta_R_1 = rdcoupling(fd_1,sweep_slope,c)
delta_R_2 = rdcoupling(fd_2,sweep_slope,c)
delta_R_3 = rdcoupling(fd_3,sweep_slope,c)

V_unambiguous_1 = dop2speed(1/(2*tm),lambda(1))/2
V_unambiguous_2 = dop2speed(1/(2*tm),lambda(2))/2
V_unambiguous_3 = dop2speed(1/(2*tm),lambda(3))/2
```

```
% Probability of False Alarm/Probability of Detection %
% H0 : x=w , H1 : x=4+w %

Amp=6;                      % Amplitude of signal %
Noise_var = sqrt(2);        % Noise Variance %
Pr_f_a = 1e-6;              % Probablity of false alarm for this radar system %
T = npwgnthresh(Pr_f_a,1,'real');  % Detection SNR threshold for signal in white
Gaussian noise using Neyman-Pearson lemma %
threshold = sqrt(db2pow(T))

pfa = 0.5*erfc(threshold/Noise_var);
pd = 0.5*erfc((threshold-Amp)/Noise_var);

fprintf('%d is Probability of False Alarm .\n',pfa);
fprintf('%d is Probability of Detection .\n',pd);

noisevar_inc = 1:0.1:10;    %Noise Variance gradual increment %
noisepower = 10*log10(noisevar_inc);
pfa = 0.5*erfc(threshold./sqrt(2*noisevar_inc));

figure
semilogy(noisepower,pfa./Pr_f_a)
grid on
title('Increase in P_{FA} due to Noise Variance')
ylabel('Increase in P_{FA} (Orders of Magnitude)')
xlabel('Noise Power Increase (dB)')
```

```
%%%%%%%%%%%% LFM PULSE %%%%%%%%%%%%%

 %% if x1=s(t) & x2=s(-t) conv (x1, x2) = LFM pulse

sFMCW_1 = phased.FMCWWaveform('SweepBandwidth',10.0e6,...
   'SampleRate',20.0e6,'SweepDirection','Up',...
   'NumSweeps',1);
sFMCW_2 = phased.FMCWWaveform('SweepBandwidth',10.0e6,...
   'SampleRate',20.0e6,'SweepDirection','Down',...
   'NumSweeps',1);

sig1 = step(sFMCW_1);
sig2 = step(sFMCW_2);

T=1/10.0e6;

plot(time,real(sig2))

co= conv(real(sig1), real(sig2));
[R C]=size(co);
time= linspace(0,T,R);

plot(time,co)

% windowlength = 32;
% noverlap = 16;
% nfft = 32;
% spectrogram(co,windowlength,noverlap,nfft,sFMCW.SampleRate,'yaxis')
```

D Architecture of the Proposed FMCW Radar With Buttler Beamformer

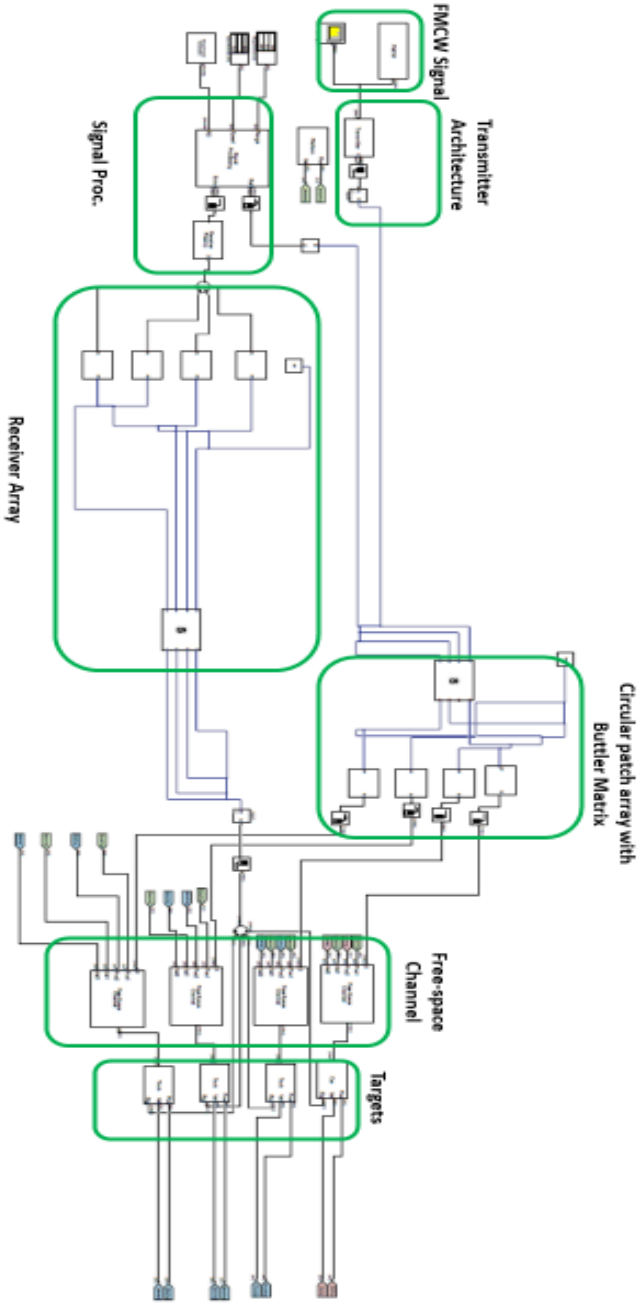

E Co-simulation in CST Software

Co-simulation simply means that a given antenna or microwave structure can be studied using an EM simulation tool or solver such as Time domain solver, Frequency domain solver, etc. which would finally give out the microwave characteristics of a certain design such as the Return loss (S_{11}), propagation properties and so forth. The software that was used for our study was CST Studio Microwave. Here are the steps for the co-simulation.

1) After the antenna design is done, we go to the Background tab (figure E-1) and we set the background material to Normal and we make sure that it is not on PEC, otherwise it could strongly bias our results.

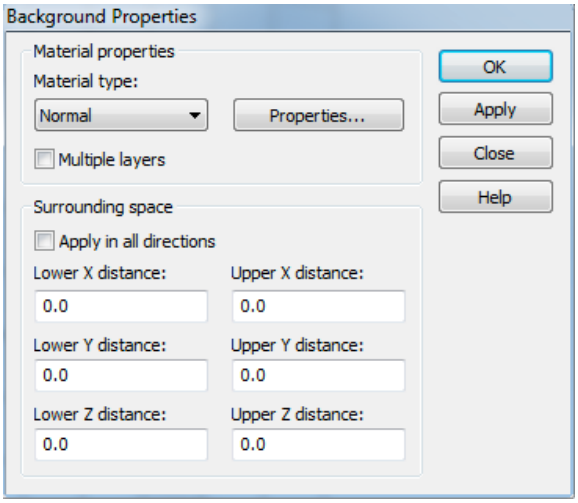

Figure E.1. Background properties tab in CST

2) Next in the Material tab as shown in figure E-2, we should set up the electric conductivity, loss tangent or thermal conductivity. We basically consider the thermal conductivity of air (background material) as 0.024 W/mK.

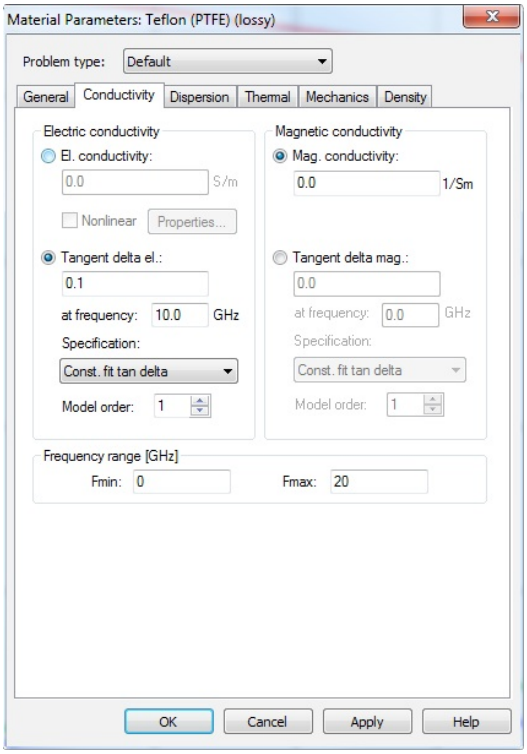

Figure E.2. Material properties tab

3) Next, we should set the boundary conditions of our structure. Under the main tab of Simulation (on the top panel of CST), we can go to the Boundary Conditions tab and choose the right boundary conditions. There are 3 options for each axis of x, y and z, which are electric, magnetic or open (add space) as we can see in figure E-3. Most of the times we just let the boundary condition be on the default case which is “open “.

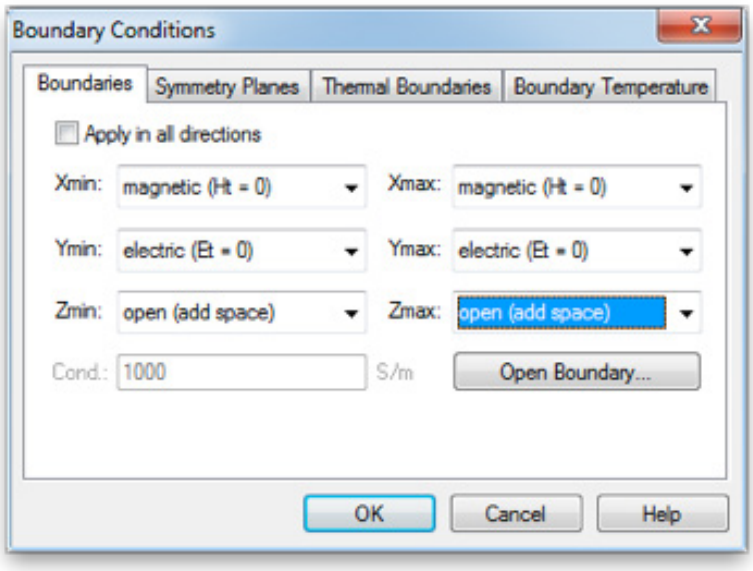

Figure E.3. Boundary conditions tab

4) In CST the excitation of structure could be done through several ways. The most common one is “waveguide port”. Waveguide ports usually show a good mode matching and also absorb the EM waves completely and thus reach high simulation accuracy. The other excitation type could be through a discrete port. A given discrete port is actually a current source with some interior resistance. To define a discrete port between two edges we need to have 2 picks which could be added under Pick Points tab. The other option for excitation of antenna, resonator, etc. is Plane Wave. As the name suggests, in this kind of excitation a plane wave that is assumed to be existing in the infinity illuminates a given structure. Usually we study RCS problems with this kind of excitation. All the 3 options are shown in figure E-4.

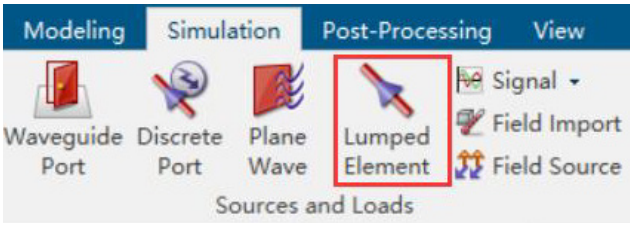

Figure E.4. Excitation ports

5) The final step for the EM section would be setting up the solver settings. In our simulations, time domain solver was used. Once we open the corresponding tab, a window such as the one on fig. 5 will pop up. The default mesh type is hexahedral.

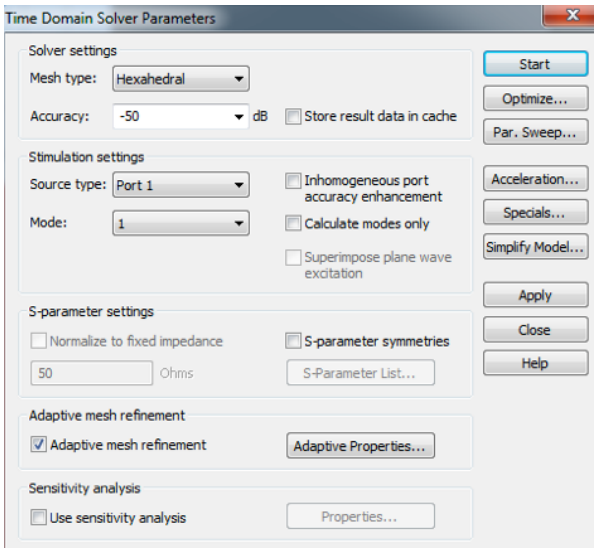

Figure E.5. Time-Domain solver

6) We can now go to the Post-Processing tab and choose thermal loss. This step would provide some initial thermal conditions for going to the next step which is running the thermal solver.
7) At this point, we are ready to run the thermal solver of CST. Thermal solvers are of 2 types of transient and stationary. Using the transient solver, one could predict the time-varying temperature behavior of a system while the stationary solver could foresee the temperature distribution of a system. We used the Thermal Stationary Solver and when we start running this solver it actually uses the thermal losses calculated in the previous step. As we can see in figure E-6, on the Thermal Stationary Solver tab we could choose the mesh type as well as the accuracy. The background temperature is considered as $273.1\,°K$.

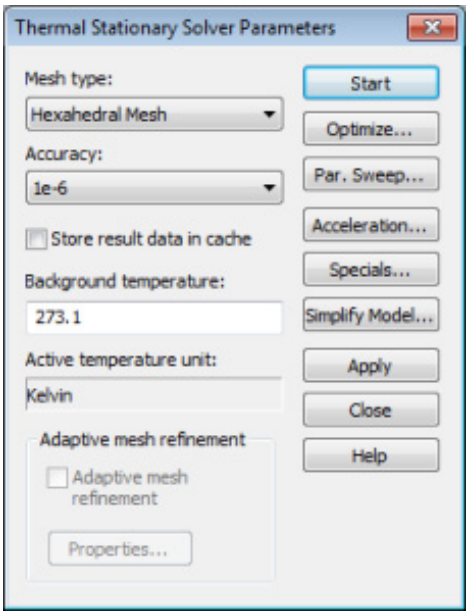

Figure E.6. Thermal stationary solver tab

8) Specific absorption ration (SAR) analysis would be the final step of the co-simulation. SAR value is expressed in $Watt/Kg$. To do that, we could open the field monitor tab and add power loss density/SAR for the favorite frequency and meanwhile under the Template-based post-processing tab, we can choose the thermal case and do the detailed setup for SAR analysis. For example, we could specify if we would want to run the average SAR or point SAR, 1g SAR or 10 g SAR.